

Received:
26 August 2018
Revised:
27 December 2018
Accepted:
18 January 2019

Cite as:
Lekan Taofeek Popoola.
Characterization and
adsorptive behaviour of snail
shell-rice husk (SS-RH)
calcined particles (CPs)
towards cationic dye.
Heliyon 5 (2019) e01153.
doi: [10.1016/j.heliyon.2019.e01153](https://doi.org/10.1016/j.heliyon.2019.e01153)



Characterization and adsorptive behaviour of snail shell-rice husk (SS-RH) calcined particles (CPs) towards cationic dye

Lekan Taofeek Popoola*

Department of Chemical and Petroleum Engineering, Afe Babalola University, Ado-Ekiti, Ekiti State, Nigeria

* Corresponding author.

E-mail address: popoolalekantaofeek@yahoo.com (L.T. Popoola).

Abstract

In this study, a low-cost composite adsorbent was prepared from snail shell and rice husk (SS-RH) through calcination for brilliant green dye (BGD) adsorption from aqueous solution. Six two-parameter and three three-parameter isotherm models were used to fit the experimental data by both linear and non-linear regression methods using ten error functions. Linear and non-linear regression analysis coupled with linear and non-linear fit error functions all revealed Langmuir and Sip as two- and three-parameter isotherm models well-fitted for BGD uptake from aqueous solution using calcined particles (CPs) of SS-RH. Chi-square (χ^2) error function proved to be the best applicable predictive error function for the two-parameter isotherm study while sum of absolute error (EABS), hybrid functional error (HYBRID) and normalized standard deviation (NSD) are the best error functions for non-linear Redlich-Peterson, Sips and Toth three-parameter isotherm models respectively. Irregular surface texture was observed for the calcined particles of SS-RH as revealed by SEM with BGD filling the opening pores after adsorption. FTIR revealed shift in spectrum broad peaks after adsorption. EDS exhibited active mixed metal oxides formation before adsorption with the observance of weight percent change after adsorption.

Keywords: Chemical engineering, Materials science

1. Introduction

Modern records have revealed worsening of ecosystems resulting from adverse effects of neo-industrial activities causing great threat to human health and the environment in which he lives. Among these is the continuous rise in the pollution of water bodies resulting from discharge of brilliant green dye from textile, printing, pharmaceutical, pulp and paper, carpet, kraft bleaching and tannery industries (Gupta et al., 1992) being assisted by the exponential rise in the world population (Foo and Hameed, 2010). Brilliant green dye (BGD) is a synthesized cationic dye with mutagenic, carcinogenic and toxic attributes causing havoc to different micro-biological species (Nandi and Patel, 2017). Thus, a proficient technique is required in the removal of BGD pollutants from water bodies as it is estimated that about 30% of dye used remains unfixed (Lakshmi et al., 2009) due to their high stability and resistance to biodegradation (El-Qada et al., 2008). A broad range of methods such as electrochemical technique (Lin and Peng, 1994), nanofiltration membranes (Ahmad et al., 2008), advanced oxidation and microfiltration (Jana et al., 2010), ultrasonic technique (Gürses et al., 2006), photocatalytic degradation (Mahalakshmi and Arabindoo, 2007), coagulation (Klimiuk et al., 1999), membrane separation (Purkait et al., 2003), merged photo-Fenton and biological oxidation (Martin and Perez, 2008), ozonation (Maldonado et al., 2006), bioremediation (Abd El-Rahim et al., 2009), aerobic degradation (Murthy and Manonmani, 2007), photo-degradation (Lodha et al., 2011) and adsorption (Nandi et al., 2009) have been proposed in treatment of waste water contaminated with dyes. However, their respective advantages and shortcomings had been presented in literatures (Can et al., 2006; Mohan et al., 2007; Basha et al., 2008; Daneshvar and Ashassi Sorkhabi Kasiri, 2004; Bayramoglu et al., 2004; Liang et al., 2009) with adsorption being considered as an outstanding method of contaminated waste water treatment (Meghea and Rehner, 1998; Panahi et al., 2008) due to its simplicity, availability, low cost, technically viable, high performance and socially satisfactory features (Nouri et al., 2007; Gottipati and Mishra, 2010).

Numerous adsorbents synthesized from low-cost natural materials such as wheat shell (Bulut and Aydin, 2006), eggshell (Akazdam et al., 2017), saw dust (Zafar et al., 2008), clay (Amin et al., 2015), bamboo charcoal (Zhu et al., 2009), guava leaf powder (Ponnusami et al., 2008), pinang frond (Ahmad and Alrozi, 2011) and so on had been used for the removal of coloured dyes from aqueous solution. In recent developments, nanocomposite iron-based adsorbent had been used for methylene blue and malachite green dyes (Alqadami et al., 2018), brown macroalga for methylene blue dye (Daneshvar et al., 2017), starch/poly(alginic acid-*cl-*

acrylamide) nanohydrogel for coomassie brilliant blue R-250 dye ([Sharma et al., 2017](#)), amberlite IRA-938 resin for rose Bengal dye ([Naushad et al., 2016](#)), polyaniline Zr(IV) selenotungstophosphate nanocomposite for methylene blue and malachite green dyes ([Pathania et al., 2015](#)), potassium hydroxide-treated palm kernel shell for methyl violet dye ([Ming-Twanga et al., 2017](#)) and nanostructured TiO₂/polyaniline nanocomposite for methyl orange and methylene blue dyes ([Gnanasekaran et al., 2018](#)) removal from aqueous solution.

In general, information obtained from simulation results of equilibrium isotherms of adsorption using experimental data is very imperative. Adsorption isotherms explain pollutants interaction with the used adsorbent at constant temperature. Parameters obtained from this are very crucial as they are applicable for (1) adsorption mechanism pathways optimization (2) adsorption systems effective design purposes and (3) surface properties and adsorbents capacities expression ([El-Khaiary, 2008](#); [Thompson et al., 2001](#)). To achieve these, the use of error analyses is required for accurate and consistent adsorption parameters prediction to enable adequate adsorption equilibrium correlations establishment ([Srivastava et al., 2006](#)). Nevertheless, data obtained from series of batch adsorption experiments have discrepancies resulting from measurement error which in return affect data accuracy. Thus, statistical error functions are effective tools to tackle great challenges of data errors to affirm accurate measurement results and better fitness of equation to experimental data.

Recently, rice husk was used as adsorbents for acidic dye removal from aqueous solution ([Edokpayi et al., 2018](#)). However, this novel study reveals the effectiveness of composite snail shell-rice husk as adsorbent for brilliant green dye uptake from aqueous solution which is a cheaply available low-cost adsorbent that could be beneficial to small scale industries for waste water treatment before disposal. Also, this research work exhibits not only best-fit isotherm model for the obtained experimental data but also best error function that gives highest efficiency of experimental data. These will be of immeasurable benefits to prospective researchers in the fields of equipment design (adsorption column) for waste water treatment and material science with specialization on generating useful materials from dumped wastes such that new theories and innovations can be developed in these areas of research.

In this study, a low-cost composite adsorbent prepared from snail shell and rice husk (SS-RH) was used for the adsorption of brilliant green dye (BGD) from aqueous solution. Two-parameters (Freundlich, Langmuir, Temkin, Dubinin-Radushkevich, Harkin-Jura and Halsey) and three-parameters (Redlich-Peterson, Sips and Toth) isotherm models were used to fit the experimental data. Because of the main shortcomings of linear regression method in fitting model and its parameters evaluation which include: (1) error changes discrepancy ([Kumar and Sivanesan, 2006](#)) and (2) unsuitability for models with more than two parameters ([Kumar 2007](#)), both linear and non-linear regression methods were used to test the fitness of these models

and their parameters evaluation using nonlinear chi-square test (χ^2), sum of squares of the errors (SSE), average relative error (ARE), residual root mean square error (RMSE), coefficient of determination (R^2), standard deviation of relative errors (S_{RE}), Marquardt's percent standard deviation (MPSD), normalized standard deviation (NSD), hybrid functional error (HYBRID), sum of absolute error (EABS) and Spearman's correlation coefficient (r_s) error functions. These error functions were minimized while R^2 was maximized simultaneously over examined concentration range to obtain best experimental data fitness and estimation of models coefficients using Microsoft Excel® solver Add-Ins.

2. Materials and methods

2.1. Preparation of calcined particles of SS-RH composite

The rice husk and snail shell were obtained as wastes from Lafenwa market, Abeokuta, Ogun State and Bodija international market, Ibadan, Oyo State, Nigeria respectively. The snail shell was soaked for some hours and unwanted materials were removed after which it was washed with distilled water for purification. The rice husk was sieved and handpicked to remove dirt and unnecessary materials. Both raw materials were oven dried at 100 °C for 24 hours. Mechanical grinder and sieve were used to obtain less than 0.4 mm particle size. The powder form of each of the raw materials was kept in separate clean polythene bag to avoid moisture contamination and placed in a covered bucket. A mixture of snail shell-rice husk was prepared at a ratio of 2.61 with the addition of 100 ml distilled water in a beaker to form a suspension. The mixture was filtered after being homogenised on a hot plate for 1 hour while the residue was placed in an oven to eliminate excess water for 2 hours at a temperature of 130 °C. The mixture was calcined at 681.10 °C for 2.61 hour in a muffle furnace (Carbolite, ELF11/6B, S/N 21-403009, United Kingdom) to obtain the composite adsorbent.

2.2. Preparation of brilliant green dye solution

The adsorbate (brilliant green dye) used in this work was purchased from TopJay Scientific Laboratory, Ajilosun, Ado-Ekiti, Ekiti State with the following physico-chemical properties: chemical formulae $C_{27}H_{33}N_2\cdot HO_4S$, molar mass 482.64 g/mol, melting point 210 °C, maximum wavelength 625 nm and solubility in water to be 100 g/L at 20 °C. 1 g of brilliant green dye powder was dissolved in 1 Litre of distilled water (1000 mg/L) to make a stock solution.

2.3. Equilibrium studies of batch adsorption

The batch adsorption process was executed using a temperature-controlled magnetic heat stirrer (Stuart heat-stirrer, SB162). UV-visible spectrophotometer (Spectrumlab

752s) was used to measure filtrate absorbance at maximum wavelength of 625 nm. A calibration curve was prepared by plotting absorbance measured at different initial concentrations of 20, 40, 60 and 80 mg/L of BGD against each other to determine adsorbate concentration. The adsorption capacity of the adsorbent, q_e (mg/g) at equilibrium is measured using Eq. (1).

$$q_e = (C_o - C_e) \frac{V}{W} \quad (1)$$

where C_o and C_e are initial and final concentrations of the BGD (mg/L), V is the volume of solution (L) and W is the weight of adsorbent (g).

2.4. Characterization of calcined particles of SS-RH composite

The calcined particles of snail shell-rice husk used as adsorbent for BGD adsorption was characterized before and after the process using scanning electron microscopy (SEM-JEOL-JSM 7600F) to study its surface morphology and textural structure. The active functional groups present in the adsorbent enhancing its adsorptive characteristic for BGD uptake from aqueous solution was characterized by Fourier transform infrared (FTIR) spectrometer (Nicolet iS10 FT-IR Spectrometer).

2.5. Isotherm models for adsorption equilibrium studies

Adsorption isotherms explain adsorbed molecules distribution between the liquid phase and the solid phase when the adsorption process reaches an equilibrium state. Table 1 summarizes all the isotherm and kinetic models used. The isotherm models used to fit the experimental data include two-parameters (Freundlich, Langmuir, Temkin, Dubinin-Radushkevich, Harkin-Jura and Halsey) and three-parameters (Redlich-Peterson, Sips and Toth) isotherm models. Pseudo-first and pseudo-second order kinetic models were used to study the progress of the reaction.

2.6. Error functions for isotherm parameters prediction

The list of error functions (non-linear chi-square test, sum of squares of the errors, average relative error, residual root mean square error, coefficient of determination, standard deviation of relative errors, Marquardt's percent standard deviation, normalized standard deviation, hybrid functional error, sum of absolute error and Spearman's correlation coefficient) used for this study is presented in Table 2. Non-linear chi-square test is calculated via summation of squares differences between experimental and calculated data with each squared difference divided by its corresponding value. Sum of squares of the errors is obtained by summing the squares of the difference between experimental and calculated value for the number of data points considered. The residual root mean square error is used to judge equilibrium model with optimal magnitude. The coefficient of determination, R^2 , gives

Table 1. Equilibrium isotherm and kinetics models used for the BGD uptake onto SS-RH.

Models	Linear models	Non-linear models	Plot	Slope and intercept	References
Two-parameter isotherms					
Freundlich	$\log q_e = \log K_F + \frac{1}{n} \log C_e$	$q_e = K_F C_e^n$	$\log q_e$ vs $\log C_e$	Slope = $1/n$, Intercept = $\log K_F$	Piccin et al. (2011)
Langmuir	$\frac{C_e}{q_e} = \frac{1}{K_L q_{\max}} + \frac{C_e}{q_{\max}}$ $R_L = \frac{1}{1 + K_L C_o}$	$q_e = \frac{q_{\max} K_L C_e}{1 + K_L C_e}$	$\frac{C_e}{q_e}$ vs C_e	Slope = $\frac{1}{q_{\max}}$, Intercept = $\frac{1}{(K_L q_{\max})}$	Langmuir (1918)
Temkin	$q_e = b_T \ln A_T + b_T \ln C_e$	$q_e = \frac{RT}{b_T} \ln A_T C_e$	q_e vs $\ln C_e$	Slope = b_T , Intercept = $b_T \ln A_T$	Temkin and Pyzhev (1940)
Dubinin- Radushkevich	$\ln(q_e) = \ln(q_m) - B_D e^2$ $e = RT \ln \left(1 + \frac{1}{C_e} \right)$ $E = \frac{1}{\sqrt{(-2B_D)}}$	$q_e = (q_m) \exp(-B_D e^2)$	$\ln q_e$ vs $\left[\ln \left(1 + \frac{1}{C_e} \right) \right]^2$	Slope = $-B_D (RT)^2$, Intercept = $\ln(q_m)$	Dubinin (1960), Hobson (1969)
Harkin-Jura	$\frac{1}{q_e^2} = \frac{B_{HJ}}{A_{HJ}} - \left(\frac{1}{A_{HJ}} \right) \log C_e$	$q_e = \left(\frac{A_{HJ}}{B_{HJ} - \log C_e} \right)^{\frac{1}{2}}$	$\frac{1}{q_e^2}$ vs $\log C_e$	Slope = $- \left(\frac{1}{A_{HJ}} \right)$, Intercept = $\frac{B_{HJ}}{A_{HJ}}$	Almeida et al. (2009)
Halsey	$\ln q_e = \frac{1}{n_H} \ln K_H - \frac{1}{n_H} \ln C_e$	$q_e = \exp \left(\frac{\ln K_H - \ln C_e}{n_H} \right)$	$\ln q_e$ vs $\ln C_e$	Slope = $- \frac{1}{n_H}$, Intercept = $\frac{1}{n_H} \ln K_H$	Tahir et al. (2010)
Three-parameter isotherms					
Redlich-Peterson	$\ln \left(K_{RP} \frac{C_e}{q_e} - 1 \right) = \beta_{RP} \ln C_e + \ln a_{RP}$	$q_e = \frac{K_{RP} C_e}{1 + a_{RP} C_e^{\beta_{RP}}}$	$\ln \left(K_{RP} \frac{C_e}{q_e} - 1 \right)$ vs $\ln C_e$	Slope = β_{RP} , Intercept = $\ln a_{RP}$	Redlich and Peterson (1959)

(continued on next page)

Table 1. (Continued)

Models	Linear models	Non-linear models	Plot	Slope and intercept	References
Sips	$\ln\left(\frac{q_e}{q_m - q_e}\right) = \frac{1}{n} \ln(C_e) + \ln(b_s)n$	$q_e = \frac{\frac{1}{n}}{\frac{q_m b_s C_e^n}{1 + b_s C_e^n}}$	$\ln\left(\frac{q_e}{q_m - q_e}\right)$ vs $\ln C_e$	Slope = $\frac{1}{n}$, Intercept = $\ln(b_s)n$	Sips (1948)
Toth	$\ln\left(\frac{q_e^{n_t}}{q_m^{n_t} - q_e^{n_t}}\right) = n_t \ln C_e + n_t \ln K_t$	$q_e = \frac{q_m K_t C_e}{(1 + (K_t C_e)^{n_t})^{n_t}}$	$\ln\left(\frac{q_e^{n_t}}{q_m^{n_t} - q_e^{n_t}}\right)$ vs $\ln C_e$	Slope = n_t , Intercept = $n_t \ln K_t$	Toth (1971)
Kinetic models					
Pseudofirst-Order	$\ln(q_e - q_t) = \ln q_e - k_1 t$	-	$\ln(q_e - q_t)$ vs t	Slope = $-k_1$, Intercept = $\ln q_e$	Lagergren (1898)
Pseudosecond-Order	$\frac{t}{q_t} = \frac{1}{k_2 q_e^2} + \frac{t}{q_e}$	-	$\frac{t}{q_t}$ vs t	Slope = $\frac{1}{q_e}$, Intercept = $\frac{1}{k_2 q_e^2}$	Cheung et al. (2001)

q_e (mg g⁻¹): experimental adsorption capacity of SS-RH adsorbent at equilibrium, K_F (mg^{1-1/n} L^{1/n} g⁻¹): Freundlich isotherm constant related to the sorption capacity, C_e (mg L⁻¹): BGD adsorbate equilibrium concentration, n : a constant which gives an idea of the grade of heterogeneity, K_L (L mg⁻¹): Langmuir constant related to the affinity of the binding sites and the energy of adsorption, C_o (mg L⁻¹): highest initial adsorbate concentration, R_L : dimensionless Langmuir equilibrium parameter, q_m (mg g⁻¹): maximum monolayer adsorption capacity of the SS-RH adsorbent, R (8.314 J mol⁻¹ K⁻¹): universal gas constant, T (°K): absolute temperature, b_T (J mol⁻¹): Temkin constant related to heat of adsorption, A_T (L mg⁻¹): equilibrium binding constant corresponding to the maximum binding energy, B_D (mol² kJ⁻²): Dubinin-Radushkevich isotherm constant of adsorption energy, ϵ : Polanyi potential related to the equilibrium concentration, E (kJ mol⁻¹): mean free energy of adsorption, A_{HJ} and B_{HJ} : Harkin-Jurah adsorption constants; K_H and n_H : Halsey isotherm constants; K_{RP} (L/g): Redlich-Peterson isotherm constant, a_{RP} (L/mg): Redlich-Peterson isotherm constant, β : Redlich-Peterson exponent which lies between 0 and 1, b_s : Sips isotherm constant related to energy of adsorption, K_t : Toth model adsorption isotherm constant, n_t : Toth model exponent, q_t (mg g⁻¹): equilibrium adsorption uptake at time, t , k_1 (min⁻¹): pseudo-first-order rate constant of adsorption, k_2 (g mg⁻¹ min⁻¹): pseudo-second-order rate constant of adsorption.

Table 2. List of error functions.

Error function	Abbreviation	Model	Reference
Nonlinear chi-square test	χ^2	$\chi^2 = \sum_{i=1}^n \frac{(q_{e,exp} - q_{e,calc})^2}{q_{e,exp}}$	Ho et al. (2002), Boulinguez et al. (2008)
Sum of squares of the errors	SSE	$SSE = \sum_{i=1}^n (q_{e,exp} - q_{e,calc})^2$	Kumar and Sivanesan (2006)
Average relative error	ARE	$ARE = \frac{100}{n} \sum_{i=1}^n \left \frac{q_{e,exp} - q_{e,calc}}{q_{e,exp}} \right $	Subramanyam and Das (2014)
Residual root mean square error	RMSE	$RMSE = \sqrt{\frac{1}{n-2} \sum_{i=1}^n (q_{e,exp} - q_{e,calc})^2}$	Vijayaraghavan et al. (2006)
Coefficient of determination	R^2	$R^2 = \frac{\sum (q_{e,exp} - \bar{q}_{e,calc})^2}{\sum (q_{e,exp} - \bar{q}_{e,calc})^2 + \sum (q_{e,exp} - q_{e,cal})^2}$	Marquardt (1963)
Standard deviation of relative errors	S_{RE}	$S_{RE} = \sqrt{\frac{\sum_{i=1}^n [(q_{e,exp} - q_{e,calc}) - ARE]^2}{n-1}}$	Marquardt (1963)
Marquardt's percent standard deviation	MPSD	$MPSD = 100 \sqrt{\frac{1}{n-p} \sum_{i=1}^n \left(\frac{q_{e,exp} - q_{e,calc}}{q_{e,exp}} \right)^2}$	Marquardt (1963)
Normalized standard deviation	NSD	$NSD = \Delta q(\%) = 100 \sqrt{\frac{1}{n-1} \sum_{i=1}^n \left(\frac{q_{e,exp} - q_{e,calc}}{q_{e,exp}} \right)^2}$	Wang et al. (2010)
Hybrid functional error	HYBRID	$HYBRID = \frac{100}{(n-p)} \sum_{i=1}^n \frac{(q_{e,exp} - q_{e,calc})}{q_{e,exp}}$	Ng et al. (2002)
Sum of absolute error	EABS	$EABS = \sum_{i=1}^n q_{e,exp} - q_{e,calc} $	Ng et al. (2003)

$q_{e,exp}$ (mg g^{-1}): value obtained from the batch experiment, $q_{e,calc}$ (mg g^{-1}): calculated value from the isotherm for corresponding $q_{e,exp}$, $\bar{q}_{e,calc}$ (mg g^{-1}): mean of $q_{e,exp}$, n: number of experimental data points, and p: number of parameters in the respective model.

the proportion of one variable variance that is predictable from the other variable and its measure allows validating the certainty of predictions made from a certain model. Hybrid functional error was developed as an improvement on sum of squares errors (SSE) at low concentrations obtained by dividing SSE value with the experimental solid-phase concentration with an inclusive divisor in the system as a term for the number of degrees of freedom (data points number minus the number of parameters within the isotherm equation). The algorithms for the simulation of linear and non-linear isotherm models using error functions with aide of Microsoft Excel® solver Add-Ins are presented as Figs. 1 and 2 respectively.

2.7. Adsorption operation parameters effect

The effects of pH (3, 5, 7 and 9), brilliant green dye initial concentration (50, 100, 150 and 200 mg/L), contact time (10, 20, 30, 40, 50 and 60 mins) and adsorbent mass (0.1, 0.2, 0.3 and 0.4 g) were investigated with the aid of a temperature controlled heat magnetic stirrer (Stuart heat-stirrer, SB162) placed at rotational speed

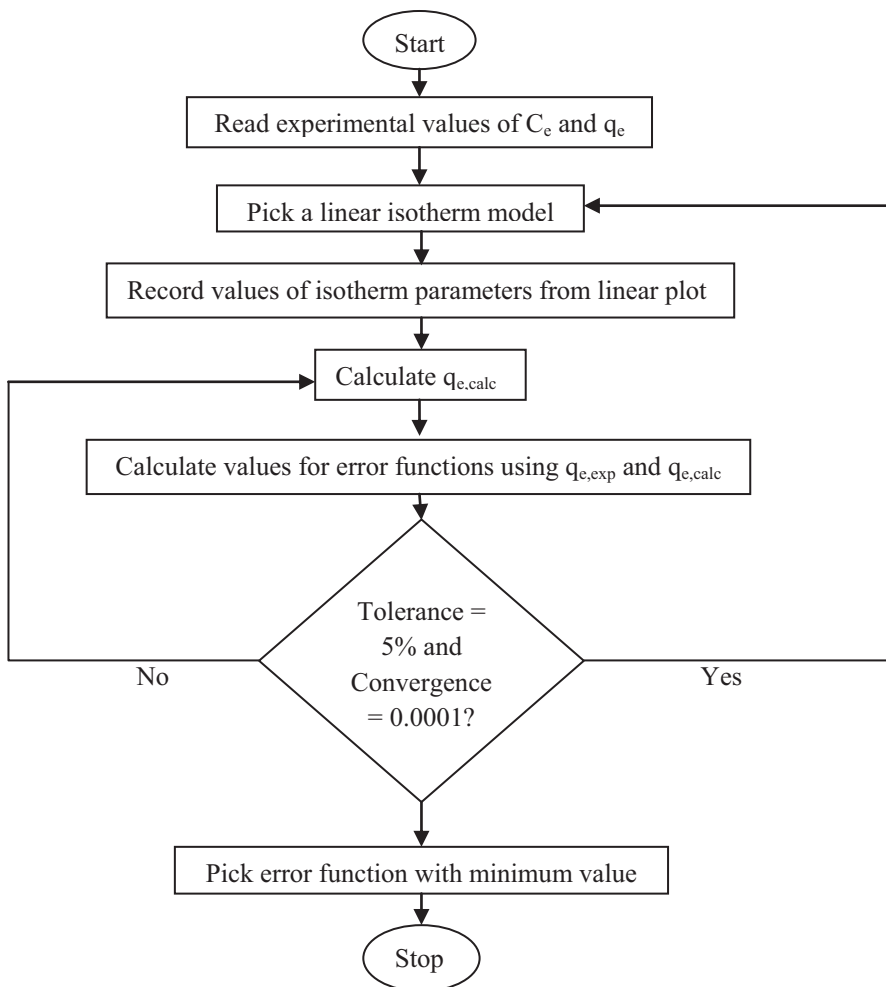


Fig. 1. Algorithm for linear isotherm models regression using error functions.

of 140 rpm. The required acidity and alkalinity were achieved using 0.1M HCl and/or 0.1M NaOH with the aid of a pH meter (OAKION, S/N 2202625, Eutech Instruments, Singapore). Initial concentration of BGD, contact time and reaction temperature were 50 mg/L, 30 mins and 50 °C respectively to study the effects of pH and mass dosage while BGD initial concentration and contact time effects were studied at constant adsorbent mass dosage of 0.2 g with unadjusted pH.

3. Results and discussion

3.1. Linear regression analysis of isotherm models

3.1.1. *Linear regression of two-parameter isotherm models*

Two-parameter adsorption isotherm constants and correlation coefficients are presented in Table 3 for BGD uptake on SS-RH at 50 °C. Previous study has shown

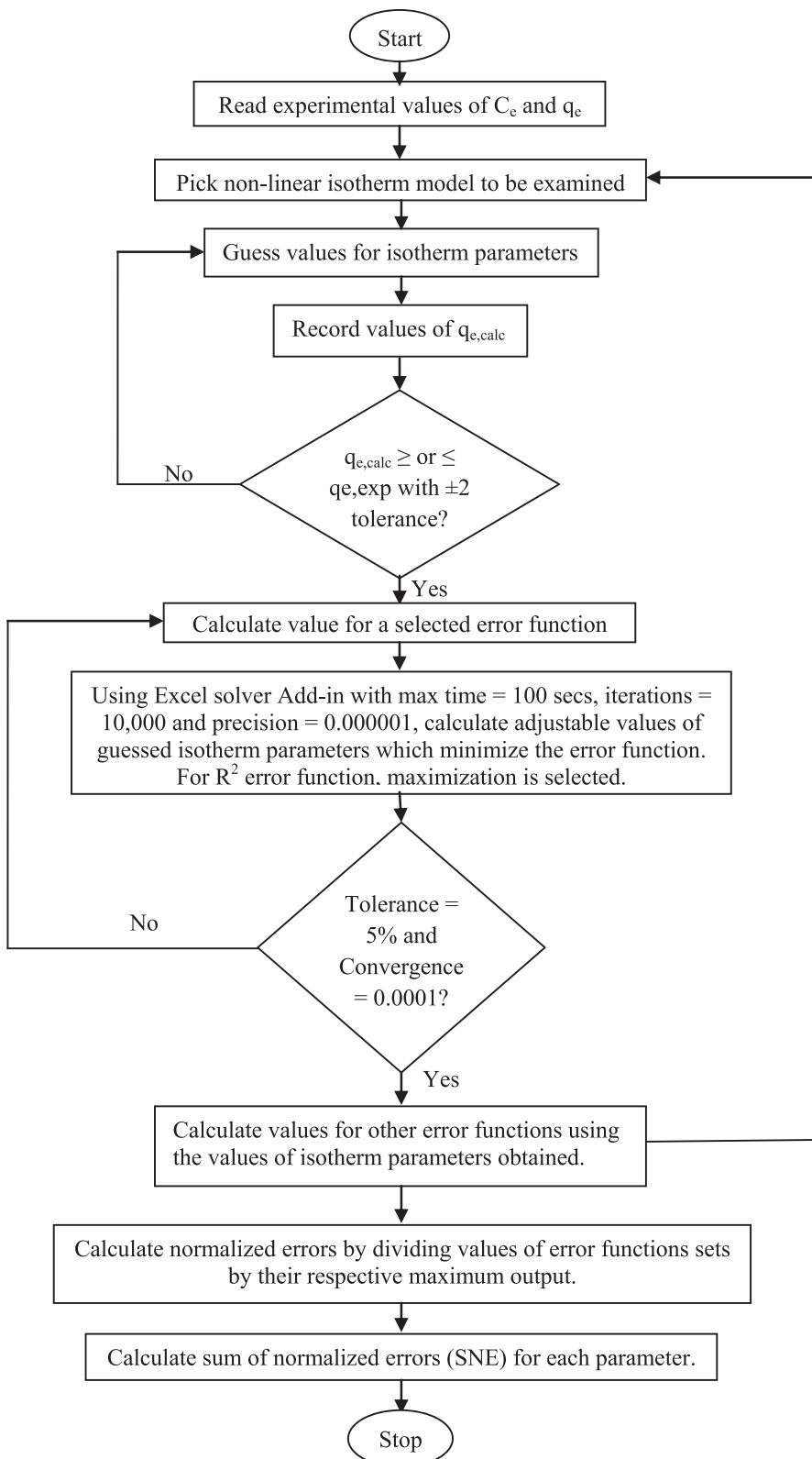


Fig. 2. Algorithm for non-linear isotherm models regression using error functions.

Table 3. Linearized and non-linearized two- and three-parameter adsorption isotherm constants and R^2 values for BGD uptake on SS-RH at 50 °C.

Isotherm models	Constants	Linearized	Non-linearized
Two-parameter isotherm models			
Freundlich	K_F ($\text{mg}^{1-1/n} \text{ L}^{1/n} \text{ g}^{-1}$) 1/n R^2	13.216 0.417 0.9519	13.0406 0.4180 0.9365
Langmuir	q_{\max} (mg g^{-1}) K_L (L mg^{-1}) R_L R^2	129.870 0.027 0.085 0.9995	131.1093 0.0260 - 0.9983
Temkin	b_T (kJ mol^{-1}) A_T (L mg^{-1}) R^2	28.886 0.248 0.9892	85.4446 0.2046 0.9802
Dubinin-Radushkevich	q_{\max} (mg g^{-1}) $B_D \times 10^{-5}$ ($\text{mol}^2 \text{ kJ}^{-2}$) E (kJ mol^{-1}) R^2	97.701 4.210 108.985 0.9451	97.8204 4.3274 - 0.9157
Harkin-Jura	A_{HJ} B_{HJ} R^2	2000.0 2.2 0.8419	2948.771 2.5227 0.0895
Halsey	n_H K_H R^2	-2.397 0.002 0.9519	10.0805 1×10^{20} 0.4257
Three-parameter isotherm models			
Redlich-Peterson	K_{RP} (L/g) a_{RP} (L/mg) β_{RP} R^2	63.7292 7.0104 0.5905 0.9755	3.0366 0.0149 1.0892 0.9996
Sips	1/n b_s (L/g) q_m (mg g^{-1}) R^2	1.1265 0.0301 123.30 1.000	1.1432 0.0185 122.1850 0.9999
Toth	n_t K_t q_m (mg g^{-1}) R^2	1.2267 0.0475 109.38 0.9503	1.2584 0.0240 120.1149 0.9999

this temperature as favourable for dye adsorption from solution (Achmad et al., 2012). Among the investigated two-parameter isotherms, a value of 0.9995 obtained for R^2 by Langmuir isotherm proved it to be well-fitted for the BGD uptake onto SS-RH. Freundlich, Temkin, Dubinin-Radushkevich, Harkin-Jura and Halsey isotherms have R^2 values of 0.9519, 0.9892, 0.9451, 0.8419 and 0.9519 respectively. In support of this, maximum monolayer adsorbent capacity (q_{\max}) value of 129.87 mg g^{-1} was predicted by Langmuir model. Recent studies also found Langmuir model to be well-fitted for adsorption process over others (Alqadami et al., 2017; Naushad et al., 2017). The linear plots for all the linearized two-parameter isotherm models are presented in Fig. 3.

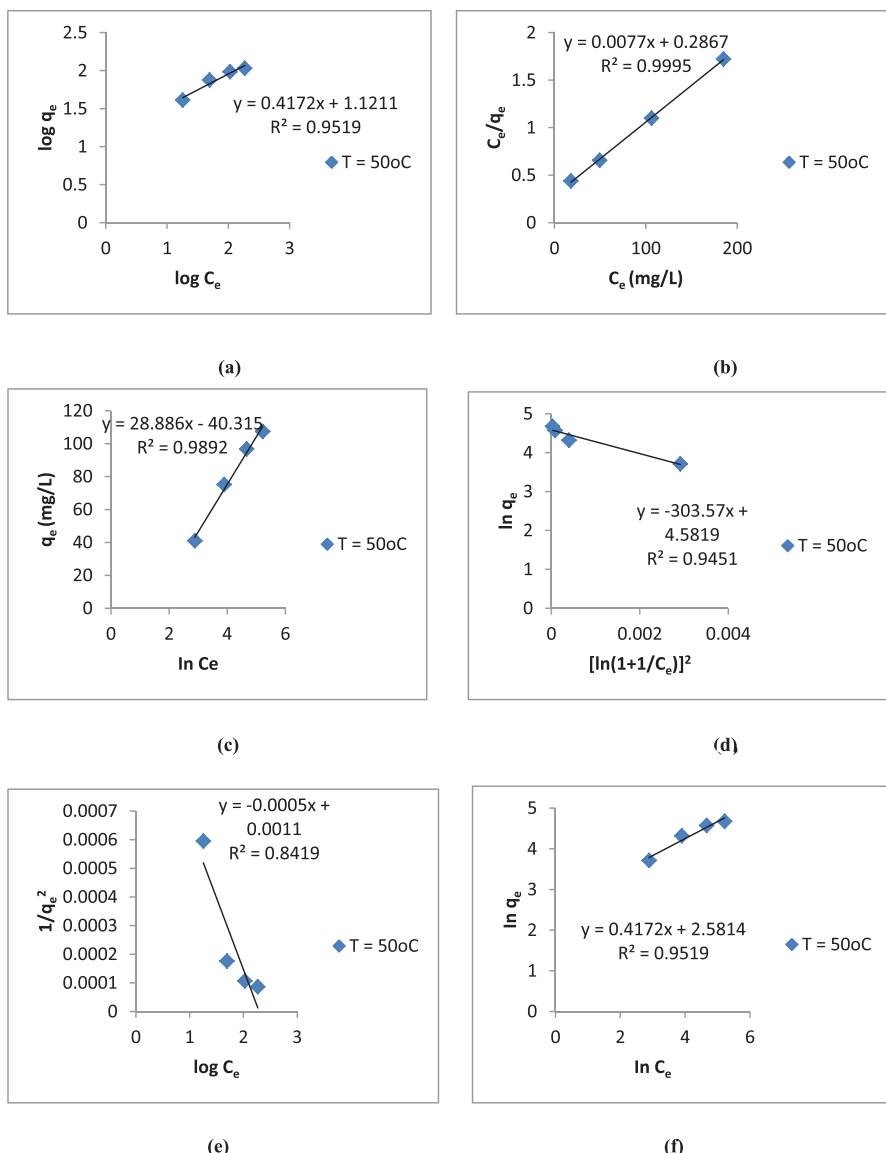


Fig. 3. Linearized two-parameter isotherm plots for (a) Freundlich (b) Langmuir (c) Temkin (d) Dubinin-Radushkevich (e) Harkins-Jura (f) Halsey.

3.1.2. Linear regression of three-parameter isotherm models

Table 3 presents three-parameter adsorption isotherm constants and correlation coefficients for BGD uptake on SS-RH at 50 °C. The Sip isotherm fitted well for the adsorption of BGD using SS-RH with R^2 value of 1.000. The R^2 values for Redlich-Peterson and Toth isotherms were 0.9755 and 0.9503 respectively. Sips isotherm had been shown by previous studies to be the most fitted three-parameter isotherm model for adsorption process. The linear plots for all the linearized three-parameter isotherm models are presented in Fig. 4.

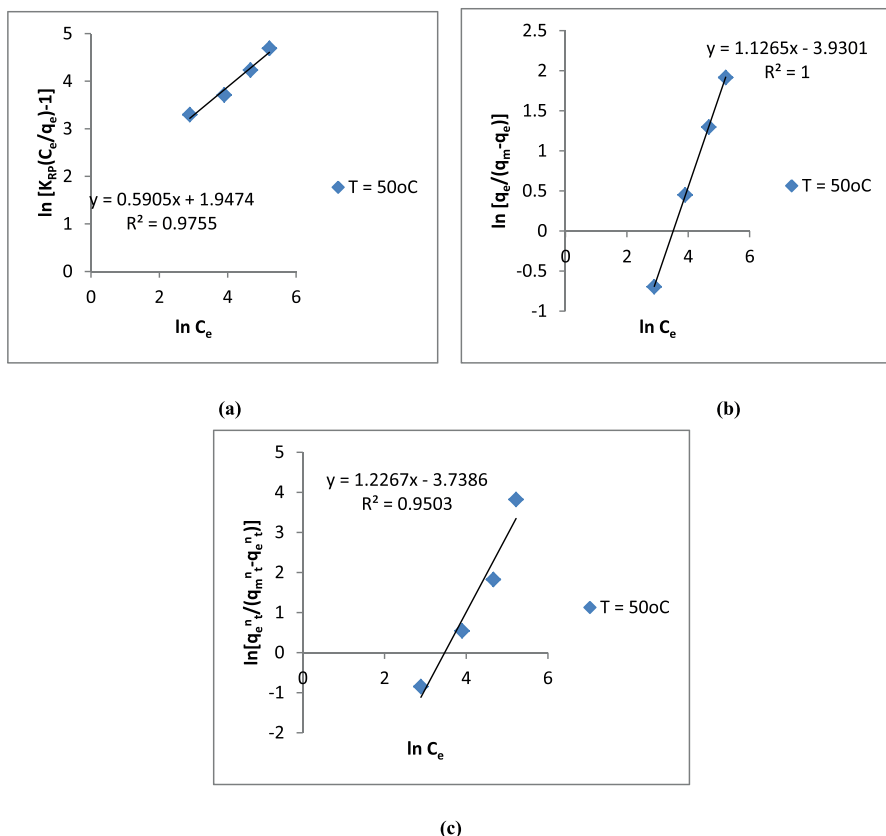


Fig. 4. Linearized three-parameter isotherm plots for (a) Redlich-Peterson (b) Sips (c) Toth.

3.2. Non-linear regression analysis of isotherm models

3.2.1. Non-linear regression of two-parameter isotherm models

The best fit was chosen based on sum of normalized error (SNE) with minimum value. **Table 3** presents the values of isotherm constants and R^2 values obtained for each two-parameter isotherm models. The values were then used to calculate adsorption capacity of SS-RH adsorbent at equilibrium (q_e) plotted against BGD adsorbate equilibrium concentration (C_e) presented as **Fig. 5**. The R^2 values revealed Langmuir to be two-parameter isotherm model that best describes adsorption of BGD onto SS-RH. The increasing order of best fit is Langmuir > Temkin > Freundlich > Dubinin-Radushkevich > Halsey > Harkin-Jura with R^2 values of $0.9983 > 0.9802 > 0.9365 > 0.9157 > 0.4257 > 0.0895$ which is the same as that obtained for the linear regression. Nevertheless, values of isotherm constants obtained for the non-linear regression are very close to those of linear regression which shows the efficacy of the non-linear isotherm models. The quantity of adsorbed BGD onto SS-RH increases with the initial concentration of BGD as shown in **Fig. 5**. This is an indication of the existence of greater affinity for BGD by the calcined SS-RH particles ([Nandi et al., 2009](#)). However, the Halsey plot revealed a reverse order as the

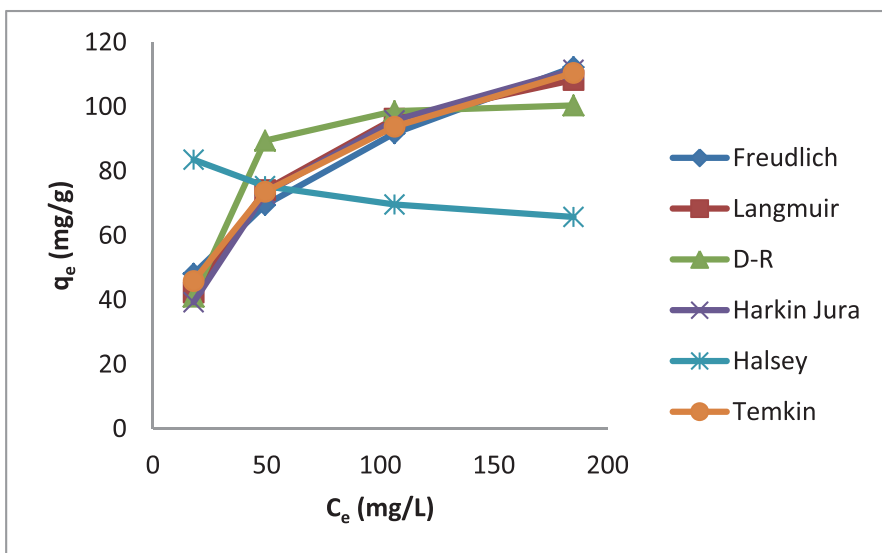


Fig. 5. Non-linearized regression of two-parameter isotherm models for BGD adsorption onto SS-RH.

amount of BGD adsorbed decreases with increase in initial concentration of the BGD which suggests that an increase in dye concentration increases number of BGD ions present in solution with limited number of active sites (Gottipati and Mishra, 2010). Nevertheless, a poor R^2 value of 0.4257 obtained for Halsey does not make this exhibition to be justifiable in driving at this conclusion.

3.2.2. Non-linear regression of three-parameter isotherm models

The sum of normalized error with minimum value was also used here in selecting the best fit for the non-linear regression of three-parameter isotherm models. The values of isotherm constants and R^2 values obtained are presented in Table 3 while the plots of adsorbed quantity of BGD by calcined SS-RH particles (q_e) with initial BGD concentrations (C_e) for all the three-parameter isotherm models are shown in Fig. 6. The R^2 values being very close to unity proved all the three-parameter isotherm models to be best fit for the BGD adsorption using SS-RH. However, Sips and Toth are the best fit with R^2 value of 0.9999. The linear regression revealed only Sips to be the best three-parameter isotherm model with R^2 value of 1.0000 with very close values of isotherm constants as obtained for the non-linear regression. In all the plots shown in Fig. 6, L-type shape was obtained indicating that adsorbed quantity of BGD onto SS-RH increases with BGD initial concentration (Giles et al., 1974). Nevertheless, it shows the efficacy of the calcined SS-RH adsorbent to adsorb BGD even at higher initial concentrations. This is also supported by increased in driving force for mass transfer at higher concentrations (Tehrani-Bagha et al., 2011).

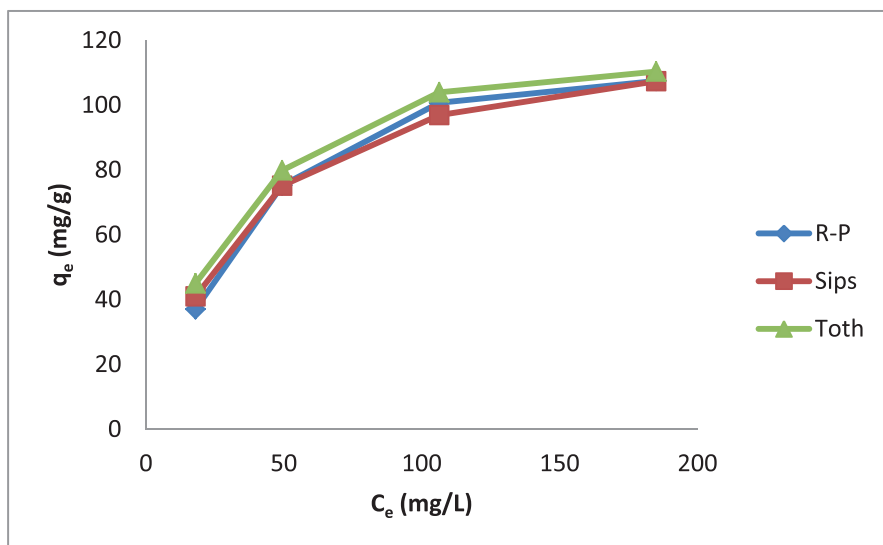


Fig. 6. Non-linearized regression of three-parameter isotherm models for BGD adsorption onto SS-RH.

3.3. Error analysis

3.3.1. Results of error functions for linear fit

In order to obtain an isotherm model that best describes the equilibrium relationship of BGD removal from aqueous solution using SS-RH, the use of error functions for the linearized isotherm models for best fit determination is imperative. Though linearized form of isotherm models have been attributed with some anomalies of error deviation, they are needed for comparative purposes with the non-linear types (Subramanyam and Das, 2009). Table 4 presents the values obtained from the simulation of error functions using linearized isotherm models of two- and three parameters. The result revealed Langmuir isotherm model to be the best two-parameter model fit for BGD uptake from aqueous solution using SS-RH having highest R^2 value of 0.9984 and lowest values for the error functions while Sips is the best three-parameter isotherm model that best describes the adsorption process with highest R^2 value of 0.9999 and lowest error functions values. The order of best fit for two-parameter isotherm models is Langmuir > Temkin > Freundlich > Halsey > D-R > H-J while the order is Sips > Toth > R-P for three-parameter models. Nevertheless, of all the error functions used, chi-square was the best error method that can accurately determine isotherm model parameters as it gave the lowest error value of 0.0770 and 0.0028 for two- and three-parameters isotherm models respectively (Ncibi, 2008). The error functions results obtained also corroborate with the linear regression analysis for the isotherm models (shown in Table 3) as both Langmuir and Sips were revealed to be the best model describing BGD adsorption from aqueous solution using SS-RH composite adsorbents. Previous studies have also presented similar results [(Bera et al., 2013), (Hamdaoui and Naffrechoux, 2007)].

Table 4. Error functions for linear regression.

Model	Error functions									
	R ²	χ ²	SSE	ARE	RMSE	S _{RE}	MPSD	NSD	HYBRID	EABS
Two-parameters isotherm models										
Freundlich	0.9362	2.0628	175.9846	7.8095	9.3804	11.8105	11.4960	9.3865	15.6190	24.5745
Langmuir	0.9984	0.0770	4.1280	1.5594	1.4367	2.3216	2.8354	2.3151	3.1188	3.7698
Temkin	0.9893	0.3743	27.9383	3.6273	3.7375	5.2184	5.3996	4.4088	7.2547	10.4705
D-R	0.9143	2.7626	241.9271	7.0652	10.9983	11.7803	12.7627	10.4207	14.1305	24.2266
H-J	0.8617	5.0446	422.7903	12.5909	14.5394	21.8056	18.1083	14.7854	25.1818	39.4935
Halsey	0.9325	2.1602	186.9215	7.9017	9.6675	12.8670	11.8114	9.6439	15.8033	24.5931
Three-parameters isotherm models										
R-P	0.7039	38.4831	3347.598	34.0905	40.9121	13.0308	68.9862	39.8292	136.3618	109.808
Sips	0.9999	0.0028	0.2185	0.2892	0.3306	0.5713	0.6549	0.3781	1.1566	0.8494
Toth	0.8752	8.0441	389.1901	14.6936	13.9497	19.0037	42.1909	24.3589	58.7745	32.1797

Bolded values indicate justification for isotherm model best fit.

3.3.2. Error functions results for non-linear fit

The results of different error functions used for the non-linear regression of two- and three-parameter isotherm models are presented in Table 5. It was observed that different error functions have different lowest sum of normalized error (SNE) values for different isotherm models. Among the two-parameter isotherm models studied, chi-square (χ^2) error function revealed parameter set with minimum SNE in three out of the six models investigated. HYBRID error function produced parameter set with lowest and highest SNE values of 3.309937 and 7.575291 respectively occurring in two out of the six two-parameter models examined. Thus, χ^2 proved to be the best applicable predictive error function for the two-parameter isotherm study of BGD adsorption onto SS-RH. However, highest R^2 value of 0.9984 obtained revealed non-linear Langmuir isotherm model to be the best fit for the adsorption process. The order of R^2 values obtained is $0.9984 > 0.9893 > 0.9510 > 0.9183 > 0.9162 > 0.5000$ for non-linear Langmuir, Temkin, Freundlich, Dubinin-Radushkevich, Harkin-Jura and Halsey isotherms respectively. The results of the error functions for linear fit also revealed Langmuir isotherm model to be the best fit with same R^2 value of 0.9984. Nevertheless, almost same order was obtained for the remaining two-parameter isotherm models. In support of these, the predicted values for maximum monolayer adsorption capacity of the SS-RH adsorbent (q_{max}) and Langmuir constant (K_L) by the non-linear Langmuir isotherm model with highest R^2 value were $130.1184 \text{ mg g}^{-1}$ and 0.0267 L mg^{-1} respectively. The results of the linear experimental plot of Langmuir isotherm (presented in Table 3) revealed approximately same results of $129.870 \text{ mg g}^{-1}$ and 0.027 L mg^{-1} for q_{max} and K_L respectively. Ghaffari et al. (2017) also presented similar results revealing same isotherm parameter values for both linear and non-linear Langmuir isotherm as the best fit. This affirms linear and non-linear Langmuir isotherm model to be the best fit of all the two-parameter isotherm models. Also, the values of isotherm parameters obtained by non-linear regression are consistent and similar to the linear transform values.

For the non-linear three-parameter isotherm models, the result (presented in Table 5) revealed EABS, HYBRID and NSD as best error function for non-linear Redlich-Peterson, Sips and Toth isotherm models respectively with respective lowest SNE values of 2.047518, 6.311617 and 3.647134. However, all the values obtained for the error functions of the linear regression of isotherm models were higher than those of the non-linear regression showing that using linear isotherm transformation is not an appropriate method in selecting a model for BGD sorption equilibria using SS-RH. However, the R^2 error function results revealed non-linear Sips isotherm model as the most appropriate three-parameter isotherm model to represent BGD adsorption using SS-RH with excellent and highest value of 1.000 as compared with non-linear Redlich-Peterson and Toth isotherm models having R^2 values of

Table 5. Error functions for non-linear regression.

Non-linear Freundlich isotherm (two-parameters)										
	R ²	χ^2	SSE	ARE	RMSE	S _{RE}	MPSD	NSD	HYBRID	EABS
K _F	16.8110	14.6012	16.8044	14.5942	16.8043	12.7044	13.0406	13.0405	16.8000	16.8101
1/n	0.3636	0.3934	0.3637	0.3824	0.3637	0.4052	0.4180	0.4180	0.3555	0.3553
R ²	0.9510	0.9465	0.9510	0.9250	0.9510	0.8887	0.9365	0.9365	0.9376	0.9376
χ^2	2.1612	1.9236	2.1595	2.6788	2.1595	4.1356	2.0641	2.0642	2.4844	2.4848
SSE	132.9008	145.8949	132.9002	215.2372	132.9002	348.1378	175.1534	175.1561	173.6063	173.4964
ARE	8.6888	8.1153	8.6865	7.8935	8.6865	8.2587	7.7272	7.7272	8.5183	8.5212
RMSE	8.1517	8.5409	8.1517	10.3739	8.1517	13.1935	9.3582	9.3583	9.3168	9.3139
S _{RE}	12.2647	11.2266	12.2510	8.0277	12.2510	7.1501	11.0980	11.0981	9.7000	9.7086
MPSD	14.2800	11.9961	14.2685	13.2703	14.2685	15.7961	11.4238	11.4239	14.2102	14.2189
NSD	11.6596	9.7948	11.6502	10.8351	11.6502	12.8975	9.3275	9.3275	11.6026	11.6097
HYBRID	17.3777	16.2306	17.3731	8.2302	17.3731	16.5175	1.3052	1.3053	17.0367	2.4828
EABS	22.7673	23.7201	22.7690	23.3701	22.7690	28.3091	24.6054	24.6056	22.5702	22.5670
SNE	8.134475	7.666938	8.131014	7.567282	8.131014	9.418471	6.881162	6.881230	8.139603	7.303683
Non-linear Langmuir isotherm (two-parameters)										
	R ²	χ^2	SSE	ARE	RMSE	S _{RE}	MPSD	NSD	HYBRID	EABS
q _{max}	130.1184	131.1093	130.1183	134.0179	130.1183	130.0548	132.0671	132.0671	132.0671	127.6149
K _L	0.0267	0.0260	0.0267	0.0245	0.0267	0.0256	0.0254	0.0254	0.0250	0.0288
R ²	0.9984	0.9983	0.9984	0.9965	0.9984	0.9960	0.9979	0.9979	0.9972	0.9972
χ^2	0.0697	0.0620	0.0697	0.0988	0.0697	0.1275	0.0669	0.0669	0.0893	0.1710
SSE	4.0577	4.4853	4.0577	9.0354	4.0577	10.2702	5.5016	5.5016	7.2620	7.2526
ARE	1.5180	1.4061	1.5180	1.1774	1.5180	1.3674	1.3175	1.3175	1.2432	1.8453

(continued on next page)

Table 5. (Continued)

Non-linear Freundlich isotherm (two-parameters)										
	R ²	χ^2	SSE	ARE	RMSE	S _{RE}	MPSD	NSD	HYBRID	EABS
RMSE	1.4244	1.4975	1.4244	2.1255	1.4244	2.2661	1.6586	1.6586	1.9055	1.9043
S _{RE}	2.1886	2.0182	2.1884	2.2732	2.1884	1.3348	2.0077	2.0077	1.6754	3.0114
MPSD	2.6067	2.1981	2.6066	2.3610	2.6066	2.8297	2.0904	2.0904	2.3643	4.5319
NSD	2.1284	1.7947	2.1283	1.9277	2.1283	2.3105	1.7068	1.7068	1.9304	3.7003
HYBRID	3.0359	2.8122	3.0359	2.3548	3.0359	2.7347	2.6349	2.6349	2.4864	3.6907
EABS	3.8292	3.9651	3.8293	4.2383	3.8293	4.5356	4.0697	4.0697	4.2683	3.5045
SNE	6.797889	6.498436	6.797796	7.400936	6.797796	7.917252	6.572740	6.572740	6.957199	9.317985
Non-linear Temkin isotherm (two-parameters)										
	R ²	χ^2	SSE	ARE	RMSE	S _{RE}	MPSD	NSD	HYBRID	EABS
b _T	92.9657	90.6904	92.9657	86.2552	92.9658	94.1191	89.0458	89.0458	89.0458	85.4446
A _T	0.2477	0.2307	0.2477	0.2107	0.2477	0.2335	0.2206	0.2206	0.2161	0.2046
R ²	0.9893	0.9887	0.9893	0.9814	0.9893	0.9788	0.9874	0.9874	0.9869	0.9802
χ^2	0.3727	0.3417	0.3727	0.4828	0.3728	0.6732	0.3560	0.3560	0.3824	0.5110
SSE	27.9323	29.5691	27.9323	49.1090	27.9323	56.5742	32.8848	32.8848	34.2220	52.1184
ARE	3.6174	3.1797	3.6174	2.6284	3.6175	3.1506	2.8956	2.8956	2.7411	2.4217
RMSE	3.7371	3.8451	3.7371	4.9553	3.7371	5.3186	4.0549	4.0549	4.1366	5.1048
S _{RE}	5.1728	4.7553	5.1728	5.8280	5.1730	3.1244	4.7331	4.7331	4.1463	5.6542
MPSD	5.3694	4.6310	5.3694	4.9408	5.3696	6.3775	4.4894	4.4894	4.6869	5.0500
NSD	4.3841	3.7812	4.3841	4.0341	4.3843	5.2072	3.6655	3.6655	3.8268	4.1233
HYBRID	7.2349	6.3593	7.2349	5.2567	7.2350	6.3011	5.7912	5.7912	5.4821	4.8434
EABS	10.4704	10.1401	10.4704	9.4461	10.4704	10.6318	9.8908	9.8908	9.8908	9.3114

(continued on next page)

Table 5. (Continued)

Non-linear Freundlich isotherm (two-parameters)										
	R ²	χ ²	SSE	ARE	RMSE	S _{RE}	MPSD	NSD	HYBRID	EABS
SNE	8.306214	7.732511	8.306214	8.399985	8.306508	9.267340	7.621757	7.621757	7.575291	8.399462
Non-linear Dubinin-Radushkevich isotherm (two-parameters)										
	R ²	χ ²	SSE	ARE	RMSE	S _{RE}	MPSD	NSD	HYBRID	EABS
q _{max}	99.5280	97.8204	99.5280	99.3553	99.5239	87.0231	96.1365	96.1027	99.3247	101.2865
B _D × 10 ⁻⁵	4.6418	4.3274	4.6337	4.2021	4.6385	5.0114	4.1411	4.1395	4.2025	4.2959
R ²	0.9183	0.9157	0.9183	0.9144	0.9183	0.8090	0.9093	0.9091	0.9144	0.9110
χ ²	2.8724	2.7410	2.8675	2.8937	2.8702	8.6404	2.8220	2.8247	2.8893	3.1665
SSE	229.5278	237.8142	229.5287	241.9766	229.5272	726.1105	258.3910	258.8829	241.8134	254.0987
ARE	8.1621	7.5395	8.1281	6.3413	8.1498	14.7114	7.4425	7.4501	6.3370	6.8173
RMSE	10.7128	10.9045	10.7128	10.9995	10.7128	19.0540	11.3664	11.3772	10.9958	11.2716
S _{RE}	12.6733	11.8799	12.6706	12.2446	12.6744	9.6877	11.3916	11.3841	12.2209	13.6736
MPSD	13.8847	12.8393	13.8592	13.3145	13.8784	24.9099	12.6253	12.6253	13.2998	14.1616
NSD	11.3368	10.4833	11.3160	10.8712	11.3317	20.3388	10.3085	10.3085	10.8592	11.5629
HYBRID	0.7330	0.4259	0.6305	12.6827	16.2996	29.4229	14.8850	14.9001	12.6739	13.63461
EABS	24.3343	24.8338	24.2748	21.7691	24.3104	44.5320	26.0971	26.1367	21.7852	23.0323
SNE	5.378589	5.198526	5.368649	5.556628	5.905602	9.589472	5.713813	5.716522	5.552557	5.881071
Non-linear Harkin-Jura isotherm (two-parameters)										
	R ²	χ ²	SSE	ARE	RMSE	S _{RE}	MPSD	NSD	HYBRID	EABS
A _{HJ}	2916.173	3562.569	3513.921	3449.999	3399.821	2093.840	2948.771	2948.771	2948.771	2948.771
B _{HJ}	2.34 × 10 ⁵	2.5449	2.82 × 10 ⁵	2.5661	2.73 × 10 ⁵	2.5016	2.4913	2.4913	2.5227	2.5227

(continued on next page)

Table 5. (Continued)

Non-linear Freundlich isotherm (two-parameters)										
	R ²	χ ²	SSE	ARE	RMSE	S _{RE}	MPSD	NSD	HYBRID	EABS
R ²	0.9162	0.0840	0.9162	0.0863	0.9162	0.1165	0.0857	0.0857	0.0895	0.0895
χ ²	319.6541	7.0599	319.6541	7.5564	319.6541	18.9849	7.8099	7.8099	8.5318	8.5318
SSE	2580.495	28267.95	2580.490	28267.95	2580.491	28267.89	28267.94	28267.94	28267.93	28267.93
ARE	99.8399	15.5107	99.8399	14.7480	99.8399	18.9476	15.7140	15.7140	14.6957	14.6957
RMSE	35.9200	118.8864	35.9199	118.8864	35.9199	118.8863	118.8864	118.8864	118.8864	118.8864
S _{RE}	37.1976	20.1313	37.1976	16.8878	37.1976	13.6110	19.0463	19.0463	15.5278	15.5278
MPSD	141.1950	24.7931	141.1950	24.5544	141.1950	33.0002	23.4050	23.4050	24.0559	24.0559
NSD	115.2853	20.2435	115.2853	20.0486	115.2853	26.9445	19.1101	19.1101	19.6416	19.6416
HYBRID	199.6799	31.0213	199.6799	29.4960	199.6799	37.8953	31.4280	31.4280	29.3914	29.3914
EABS	320.1002	41.8594	320.1002	39.5225	320.1002	67.6869	46.7383	46.7383	42.5692	42.5692
SNE	8.393424	3.447638	8.393423	3.338546	8.393423	3.610912	3.422323	3.422323	3.309937	3.309937

Non-linear Halsey isotherm (two-parameters)										
	R ²	χ ²	SSE	ARE	RMSE	S _{RE}	MPSD	NSD	HYBRID	EABS
n _H	5.41×10^8	10.0805	9.6941	9.7544	9.6660	12.2371	10.5503	10.5503	9.7544	9.7544
K _H	1×10^{20}									
R ²	0.500	0.4257	0.3852	0.4544	0.3826	0.4907	0.4589	0.4589	0.3913	0.3913
χ ²	312.6043	62.0665	70.5855	67.8975	72.0597	132.3204	69.5309	69.5309	67.8975	67.8975
SSE	27630.97	4890.040	4254.551	4286.399	4250.795	12815.26	6475.502	6475.502	4286.399	4286.399
ARE	98.5672	43.3621	43.866	42.6491	44.4522	54.7047	44.2178	44.2178	42.6491	42.6491
RMSE	117.5393	49.4472	46.1224	46.2947	46.1020	80.0477	56.9012	56.9012	46.2947	46.2947
S _{RE}	36.9262	47.6276	58.6866	55.7017	60.1522	32.4637	39.7980	39.7980	55.7017	55.7017

(continued on next page)

Table 5. (Continued)

Non-linear Freundlich isotherm (two-parameters)										
	R ²	χ ²	SSE	ARE	RMSE	S _{RE}	MPSD	NSD	HYBRID	EABS
MPSD	139.3976	69.2279	83.7700	80.7604	85.2771	83.6452	64.1482	64.1482	80.7603	80.7603
NSD	113.8177	56.5244	68.3979	65.9406	69.6285	68.2960	52.3768	52.3768	65.9405	65.9405
HYBRID	197.1344	10.2201	87.7323	85.2983	88.9043	109.4093	88.4355	88.4355	85.2983	85.2983
EABS	316.5470	127.3641	112.2073	111.4226	112.5861	197.6429	145.5357	145.5357	111.4226	111.4226
SNE	9.613880	4.326761	4.964644	4.977089	5.022927	6.023670	4.797641	4.797641	4.850888	4.850888

Non-linear Redlich-Peterson isotherm (three-parameters)										
	R ²	χ ²	SSE	ARE	RMSE	S _{RE}	MPSD	NSD	HYBRID	EABS
K _{RP}	3.0873	3.0583	3.0873	3.4778	3.0876	3.0704	3.0396	3.0395	3.0363	3.0366
a _{RP}	0.0154	0.0147	0.0154	0.0356	0.0154	0.0154	0.0142	0.0142	0.0143	0.0149
β _{RP}	1.0804	1.0868	1.0804	0.9367	1.0804	1.0791	1.0918	1.0918	1.0893	1.0892
R ²	0.9998	0.9998	0.9998	0.9883	0.9998	0.9996	0.9998	0.9998	0.9998	0.9996
χ ²	0.0058	0.0054	0.0058	0.3183	0.0058	0.0114	0.0056	0.0056	0.0067	0.0066
SSE	0.4403	0.4646	0.4403	30.4853	0.4403	0.9410	0.5116	0.5120	0.6110	0.6118
ARE	0.4305	0.3821	0.4304	2.1645	0.4310	0.3953	0.3581	0.3579	0.3077	0.3068
RMSE	0.4692	0.4820	0.4692	3.9042	0.4692	0.6859	0.5058	0.5060	0.5527	0.5529
S _{RE}	0.6393	0.5898	0.6391	4.3220	0.6410	0.4122	0.5820	0.5821	0.6325	0.6334
MPSD	0.9238	0.8133	0.9232	5.8540	0.9257	1.1842	0.7936	0.7936	0.8653	0.8659
NSD	0.5333	0.4696	0.5330	3.3798	0.5345	0.6837	0.4582	0.4582	0.4996	0.4989
HYBRID	1.7220	1.5283	1.7216	8.6580	1.7239	1.5813	1.4325	1.4314	1.2308	1.2316
EABS	1.2464	1.2296	1.2465	7.7766	1.2459	1.3527	1.2386	1.2383	1.0878	1.0827

(continued on next page)

Table 5. (Continued)

Non-linear Freundlich isotherm (two-parameters)										
	R ²	χ^2	SSE	ARE	RMSE	S _{RE}	MPSD	NSD	HYBRID	EABS
SNE	2.174416	2.081165	2.174099	9.988498	2.175875	2.281331	2.059893	2.059722	2.048831	2.047518
Non-linear Sips isotherm (three-parameters)										
	R ²	χ^2	SSE	ARE	RMSE	S _{RE}	MPSD	NSD	HYBRID	EABS
1/n	1.1395	1.1416	1.1395	1.1395	1.1395	1.1385	1.1432	1.1432	1.1432	1.1395
b _s	0.0187	0.0186	0.0187	0.0187	0.0187	0.0187	0.0185	0.0185	0.0185	0.0187
q _m	122.3609	122.2639	122.3609	122.3605	122.3605	122.2555	122.1850	122.1850	122.1850	122.3606
R ²	1.0000	0.9999	0.9999	0.9999	1.0000	0.9999	0.9999	0.9999	0.9999	0.9999
χ^2	0.000423	0.000408	0.000423	0.000463	0.000423	0.001148	0.000415	0.000415	0.000417	0.000463
SSE	0.0371	0.0381	0.0371	0.0405	0.0371	0.0990	0.0399	0.0399	0.0400	0.0405
ARE	0.1079	0.0963	0.1079	0.0965	0.1079	0.1471	0.0905	0.0905	0.0882	0.0965
RMSE	0.1363	0.1379	0.1363	0.1423	0.1363	0.2225	0.1413	0.1413	0.1414	0.1423
S _{RE}	0.1683	0.1582	0.1682	0.1382	0.1682	0.1227	0.1555	0.1555	0.1496	0.1382
MPSD	0.2257	0.2117	0.2256	0.2327	0.2256	0.3729	0.2092	0.2092	0.2101	0.2327
NSD	0.1303	0.1222	0.1303	0.1344	0.1303	0.2153	0.1208	0.1208	0.1213	0.1344
HYBRID	0.4317	0.3853	0.4315	0.3860	0.4317	0.5885	0.3618	0.3618	0.3529	0.3860
EABS	0.3508	0.3377	0.3507	0.3442	0.3508	0.4774	0.3325	0.3325	0.3313	0.3442
SNE	6.768145	6.451951	6.766633	6.554187	6.767283	9.728955	6.372008	6.372008	6.311617	6.554187
Non-linear Toth isotherm (three-parameters)										
	R ²	χ^2	SSE	ARE	RMSE	S _{RE}	MPSD	NSD	HYBRID	EABS
n _t	1.2435	1.2521	1.2435	1.2687	1.2435	1.2392	1.2584	1.2584	1.2063	1.2286

(continued on next page)

Table 5. (Continued)

Non-linear Freundlich isotherm (two-parameters)										
	R ²	χ^2	SSE	ARE	RMSE	S _{RE}	MPSD	NSD	HYBRID	EABS
K _t	0.0242	0.0241	0.0242	0.0239	0.0242	0.0242	0.0240	0.0240	0.0239	0.0241
q _m	120.5514	120.3080	120.5517	120.0994	120.5515	120.4588	120.1148	120.1149	123.0771	121.0800
R ²	0.9999	0.9999	0.9999	0.9998	0.9999	0.9998	0.9999	0.9999	0.9995	0.9999
χ^2	0.001565	0.001486	0.001565	0.002666	0.001565	0.003033	0.001521	0.001521	0.012901	0.002588
SSE	0.1308	0.1353	0.1308	0.2581	0.1308	0.2596	0.1442	0.1442	1.2939	0.2013
ARE	0.2166	0.1913	0.2164	0.1314	0.2166	0.2164	0.1785	0.1785	0.4791	0.1946
RMSE	0.2557	0.2601	0.2557	0.3592	0.2557	0.3603	0.2685	0.2685	0.8043	0.3172
S _{RE}	0.3297	0.3061	0.3296	0.3919	0.3297	0.2281	0.3002	0.3002	1.0611	0.2627
MPSD	0.4504	0.4108	0.4502	0.5248	0.4504	0.6035	0.4040	0.4039	1.1407	0.5790
NSD	0.2600	0.2372	0.2599	0.3030	0.2600	0.3485	0.2332	0.2332	0.6586	0.3343
HYBRID	0.8662	0.7650	0.8657	0.5256	0.8662	0.8654	0.7141	0.7140	1.9162	0.7782
EABS	0.6732	0.6504	0.6730	0.5087	0.6732	0.7570	0.6433	0.6432	1.8499	0.6426
SNE	3.908702	3.702006	3.907494	3.965639	3.908702	4.469293	3.647328	3.647134	9.999599	4.172974

NB: The bolded values are the lowest values of respective error functions. Only R² have highest values.

0.9998 and 0.9999 respectively. The values of non-linear Sips isotherm parameters obtained were 1.1395, 0.0187 L/g and 122.3609 mg g⁻¹ for inverse of constant (I/n), Sips constant (b_s) and q_{max} respectively which are almost the same as 1.1265, 0.0301 L/g and 123.30 mg g⁻¹ obtained respectively for the linear plot of the Sips model (presented in Table 3). This affirms the consistency of the non-linear Sips isotherm model with the linear form. Similar studies have shown non-linear Langmuir and Sip isotherm models using parameter set obtained from MPSD error as the best overall model for all two- and three-parameter models (Ho et al., 2002; Chen, 2015).

3.4. Adsorption operational parameters effect

The adsorption capacity of calcined particles of snail shell-rice husk increases from 37.342 to 88.625 mg/g as the solution pH increases from 3 to 9 (Fig. 7a). Lower adsorption capacity at lower pH resulted from the presence of positively charged ion generated via calcination on adsorbent surface competing with the hydrogen

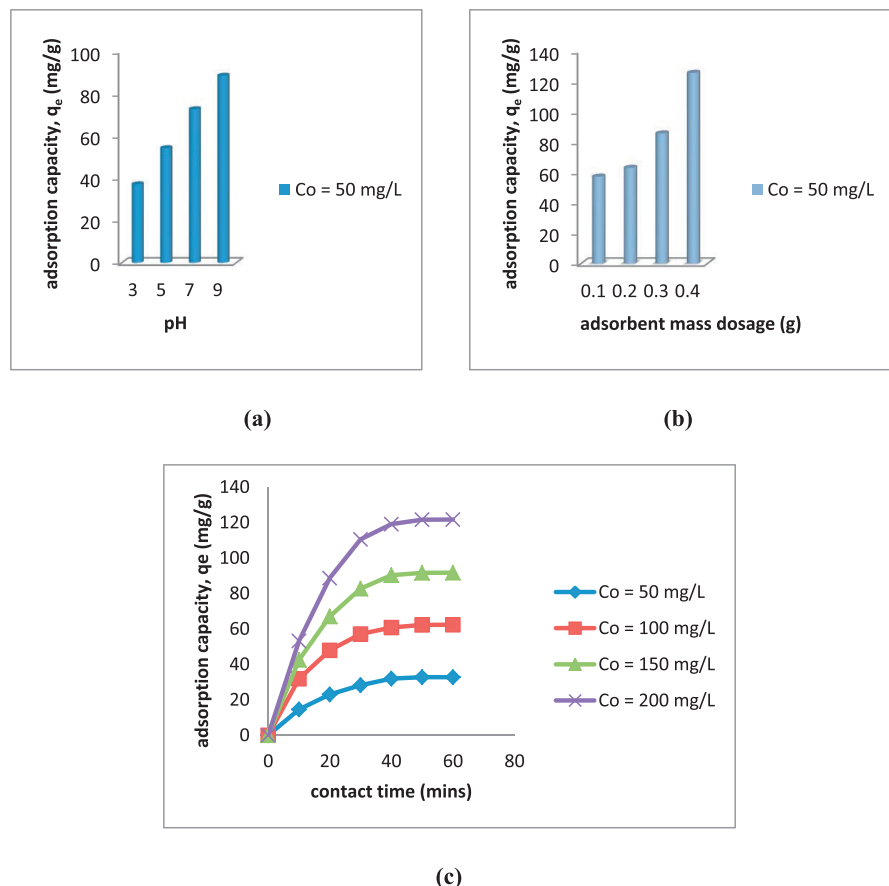


Fig. 7. Adsorption operation parameters effects for (a) BGD solution pH (b) adsorbent mass dosage (c) contact time and BGD initial concentration.

ion of the BGD. However, presence of strong electrostatic and weak van der Waals forces between the adsorbate negatively charged ions (OH^-) and adsorbent positively charged ion (H^+) accounted for higher adsorption capacity at higher pH value. This observation was also revealed by previous study (Rahman and Sathasivam, 2015).

The adsorbent adsorption capacity increases from 57.237 to 125.618 mg/g as the adsorbent mass dosage increases from 0.1 to 0.4 g (Fig. 7b). This could be attributed to formation of additional surface area for BGD removal from aqueous solution which subsequently increases the number of active sites. Similar results have been reported elsewhere (Venkatesh et al., 2010; Shirmardi et al., 2012).

As the adsorption contact time increases coupled with increase in the BGD initial concentration, the adsorption capacity also increases rapidly at the first 20 minutes of each experimental run while equilibrium was attained after 40 minutes (Fig. 7c). The adsorption process was favoured by increase in concentration gradient; and electrostatic forces between molecules of BGD and atoms on adsorbent surface. Attainment of equilibrium after 40 minutes could be attributed to decrease in active sites on adsorbent surface due to its pores being occupied by BGD causing reduction in internal diffusion. Similar studies have also reported almost same results (Ramuthai et al., 2009; Aljebori and Alshirifi, 2017).

3.5. Kinetic studies

Table 6 presents parameters obtained for the pseudo-first-order and pseudo-second-order kinetic studies of BGD uptake from aqueous solution using calcined particles of SS-RH. First order rate constant (k_1) and corresponding theoretical equilibrium adsorption capacity ($q_{e,\text{cal}}$) were respectively obtained from the intercept and slope of $\ln(q_e - q_t)$ against time. Second order rate constant (k_2) and corresponding theoretical equilibrium adsorption capacity ($q_{e,\text{cal}}$) were respectively obtained from the intercept and slope of $\frac{t}{q_t}$ against time. The R^2 values of pseudo-first-order kinetic model ranging between 0.9746 and 0.9979 for all BGD initial concentrations coupled with close margin between values of theoretical $q_{e,\text{cal}}$ and experimental

Table 6. Kinetic model parameters and R^2 values of BGD adsorption onto calcined particles of SS-RH.

C_o (mg/L)	$q_{e,\text{exp}}$ (mg/g)	Pseudo-first-order			Pseudo-second-order		
		k_1 (min^{-1})	$q_{e,\text{cal}}$ (mg/g)	R^2	k_2 ($\text{g mg}^{-1} \text{ min}^{-1}$)	$q_{e,\text{cal}}$ (mg/g)	R^2
50	37.643	$5.41*10^{-2}$	36.146	0.9944	$1.43*10^{-2}$	29.281	0.9691
100	73.094	$7.12*10^{-2}$	74.935	0.9979	$1.78*10^{-2}$	57.144	0.9492
150	91.210	$3.33*10^{-2}$	89.985	0.9831	$2.52*10^{-2}$	75.081	0.9205
200	108.291	$2.87*10^{-2}$	107.914	0.9746	$2.88*10^{-2}$	90.150	0.9879

$q_{e,\text{exp}}$ adsorption capacities at equilibrium suggest it as being the best to describe BGD adsorption onto calcined particles of SS-RH. The reaction rate was controlled by chemisorptions due to electrons exchange between BGD ions and SS-RH functional groups (Hameed et al., 2009). Also, physi-sorption of SS-RH towards BGD dye was observed to an extent (Idan et al., 2018). Previous studies have also reported similar results (Shelke et al., 2010; Amin et al., 2015). However, contrary result was presented elsewhere (Alqadami et al., 2017).

3.6. Material characterization

3.6.1. SEM images

The SEM images obtained before and after the adsorption of BGD onto calcined particles of SS-RH are presented as Fig. 8(a) and (b) respectively. Fig. 8a revealed an irregular surface texture with creation of pores resulting from the calcination of the raw composite adsorbent coupled with water liberation which allows uptake of BGD onto the surface and the pores. The SEM image shown as Fig. 8b revealed the adsorption of BGD onto the surface and opening pores of the SS-RH. Nearly all the available pores created were filled up with the BGD after the adsorption process with noticeable change in the colour of the calcined particles of SS-RH.

3.6.2. FT-IR analysis

Table 7 summarizes the values of broad peaks wavelengths with respective suggestions revealed by FT-IR spectra (Fig. 9) of the composite SS-RH adsorbent before and after the uptake of BGD respectively recorded in the range of 350–4400 nm. Observed sharp broad peaks suggested complex nature of the calcined particles of SS-RH adsorbent with the availability of active functional groups enhancing BGD adsorption onto the adsorbent surface and pores. A shift in the broad peaks of the spectrum after adsorption and the stated observations suggests functional groups presence on the SS-RH surface (Amin et al., 2015); and interaction between the

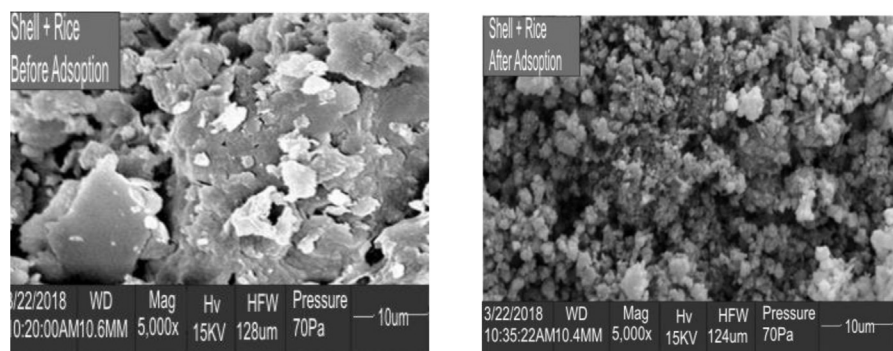
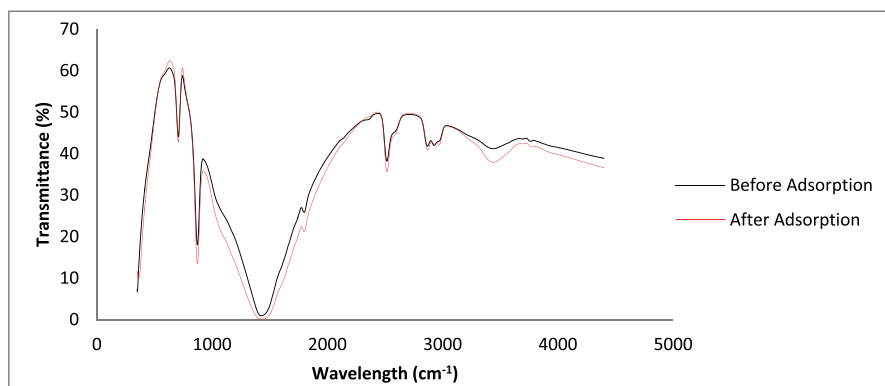


Fig. 8. SEM image of synthesized snail shell-rice husk composite adsorbent (a) before (b) after BGD adsorption.

Table 7. FTIR of SS-RH before and after BGD adsorption.

IR band	FT-IR wavelength (cm^{-1}) for SS-RH		Observations/suggestions
	Before adsorption	After adsorption	
1	3844.71	-	Stretching vibration of H_2O molecules
2	3402.00	3496.23	-OH and -NH functional groups vibration
3	2971.22	3007.62	Asymmetric stretching vibrations of the C-H bonds of the aliphatic groups
4	2799.27	2816.01	Symmetric Stretching of C-H bond
5	2549.14	2549.47	Bending vibration of C-H bond in methylene group
6	1794.62	1797.84	Stretching vibration of $-\text{C}=\text{O}$ of carboxylate groups
7	1427.63	1427.00	symmetric stretching vibration group of COO^- and aromatic rings vibrational stretching
8	878.86	878.98	S=O stretching bands of $-\text{SO}_3^-$ bonds in sulfonate groups
9	703.72	703.79	Out- of- plane bending of C-O
10	-	368.38	Bending vibration of Al—O—Si present in the rice husk

**Fig. 9.** Ftir spectra before and after BGD adsorption.

BGD molecules and the functional groups during adsorption respectively (Kooh et al., 2016).

3.6.3. Energy dispersive spectroscopy (EDS) analysis

Table 8 presents the energy dispersive spectroscopy (EDS) results revealing formation of active mixed metal oxides (Al-O, Na-O, Fe-O, Ca-O, Si-O, S-O) with different weight percent due to calcination of the SS-RH particles at higher temperature. Changes in the respective weight of the active mixed metal oxides after adsorption revealed their positive influence on the BGD adsorption on the active

Table 8. Energy dispersive spectroscopy (EDS) of SS-RH adsorbent showing weight percent of elements before and after adsorption.

Element	Wt (%) before adsorption	Wt (%) after adsorption
Sulphur	2.30	2.20
Oxygen	45.00	41.03
Aluminium	1.25	1.05
Sodium	3.70	5.10
Silicon	32.20	30.10
Calcium	10.21	15.00
Iron	3.11	3.12
Potassium	2.23	2.40

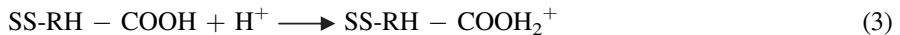
sites of calcined SS-RH particles. A study also revealed silicon and calcium composition to be 32.2 and 10.21 wt% whose sources were from rice husk and snail shell respectively (Korotkova et al., 2016). Reduction in wt% of active oxides of Si, Al and S in the calcined SS-RH particles suggested their strong affinity to adsorb BGD from aqueous solution. Though a study presented by Kumar et al. (2010) synthesized active mixed metal oxides from only rice husk for adsorption of cadmium from aqueous solution, similar weight percent were observed before and after the process.

3.7. Proposed adsorption mechanism of brilliant green dye onto calcined particles of snail shell-rice husk

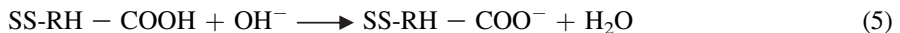
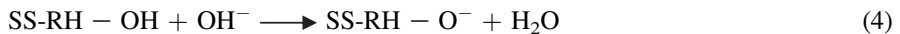
The reaction mechanism of BGD adsorption onto CPs of SS-RH is a function of electrostatic attractive force existing between negatively charged surface of the adsorbent and positively charged BGD dye. The functional groups present on the CPs of SS-RH surface and pH reliance of BGD adsorption from aqueous solution onto CPs of SS-RH are instruments for the explanation of these electrostatic attractive forces. The existence of hydroxyl (OH^-) and carboxyl (COO^-) groups on CPs of SS-RH were revealed by FTIR (Table 7) at wavelengths 3496.23 cm^{-1} and 1427.63 cm^{-1} respectively. The ionization of OH^- and COO^- groups is a function BGD solution pH which causes electrical charge on CPs of adsorbent surface. These groups on adsorbent surface can either lose or gain a proton which results to surface charge that varies with changes in BGD solution pH.

At low solution pH, protonation reaction occurs at the active sites present on CPs of SS-RH surface. Thus, the adsorbent surface is positively charged due to reaction between H^+ in solution and groups (OH^- and COO^-) on its surface as shown in Eqs. (2) and (3) below.

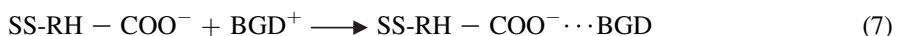
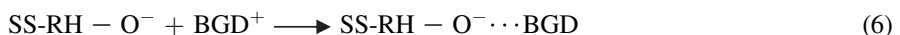




Deprotonation reaction occurs at high solution pH and the active sites on CPs of SS-RH surface are negatively charged as a result of reaction between OH^- and groups (OH^- and COO^-) on its surface as shown in Eqs. (4) and (5) below.



Eqs. (4) and (5) revealed that electrostatic attractive forces enhanced BGD adsorption onto CPs of SS-RH at high solution pH. Thus, the proposed mechanism of adsorption process can be represented as Eqs. (6) and (7).



4. Conclusion

Linear and non-linear regression of two- and three-parameter isotherm models have been investigated using different error functions for BGD removal from aqueous solution using snail shell-rice husk. Langmuir and Sip fitted well for BGD uptake from aqueous solution using SS-RH. Chi-square (χ^2) predicted well for non-linear Langmuir model while EABS, HYBRID and NSD predicted well for non-linear R-P, Sips and Toth isotherm models for BGD adsorption onto SS-RH. The SEM images before and after adsorption revealed formation of irregular surface texture and adsorption of BGD onto the surface of calcined particles of SS-RH opening pores respectively. FTIR analysis exhibited shift in the spectrum broad peaks after adsorption suggesting the presence and interaction of active functional groups on SS-RH surface with BGD molecules. EDS analysis showed the formation of active mixed metal oxides before adsorption while changes in their respective weight percent was observed after adsorption.

Declarations

Author contribution statement

Lekan T. Popoola: Conceived and designed the experiments; Performed the experiments; Analyzed and interpreted the data; Contributed reagents, materials, analysis tools or data; Wrote the paper.

Funding statement

This research did not receive any specific grant from funding agencies in the public, commercial, or not-for-profit sectors.

Competing interest statement

The authors declare no conflict of interest.

Additional information

No additional information is available for this paper.

References

- Abd El-Rahim, W.M., El-Ardy, O.A.M., Mohammad, F.H.A., 2009. The effect of pH on bioremediation potential for the removal of direct violet textile dye by *Aspergillus niger*. Desalination 249, 1206–1211.
- Achmad, A., Kassim, J., Suan, T.K., Amat, R.C., Seey, T.L., 2012. Equilibrium, kinetic and thermodynamic studies on the adsorption of direct dye onto a novel green adsorbent developed from *Uncaria gambir* extract. J. Phys. Sci. 23 (1), 1–13.
- Ahmad, A., Tan, L., Shukor, S., 2008. Dimethoate and atrazine retention from aqueous solution by nanofiltration membranes. J. Hazard. Mater. 151, 71–77.
- Ahmad, M.A., Alrozi, R., 2011. Removal of malachite green dye from aqueous solution using rambutan peel-based activated carbon: equilibrium, kinetic and thermodynamic studies. Chem. Eng. J. 171 (2), 510–516.
- Akazdam, S., Chafi, M., Yassine, W., Sebbahi, L., Gourich, B., Barka, N., 2017. Decolourization of cationic and anionic dyes from aqueous solution by adsorption on NaOH treated eggshells: batch and fixed bed column study using response surface methodology. J. Mater. Environ. Sci. 8 (3), 784–800. <http://www.jmaterenvironsci.com>.
- Aljebori, A.M.K., Alshirifi, A.N., 2017. Effect of different parameters on the adsorption of Maxilon blue GRL textile dye from aqueous solution using white marble. Int. J. Environ. Stud. 37, 1–17.
- Almeida, C.A.P., Debacher, N.A., Downs, A.J., Cottet, L., Mello, C.A.D., 2009. Removal of methylene blue from colored effluents by adsorption on montmorillonite clay. J. Colloid Interface Sci. 332, 46–53.

- Alqadami, A.A., Naushad, M., Alothman, Z.A., Ahamad, T., 2018. Adsorption performance of MOF nanocomposite for methylene blue and malachite green dyes: kinetics, isotherm and mechanism. *J. Environ. Manag.* 223, 29–36.
- Alqadami, A.A., Naushad, M., Alothman, Z.A., Ghfar, A.A., 2017. Novel metal-organic framework (MOF) based composite material for the sequestration of U(VI) and Th(IV) metal ions from aqueous environment. *ACS Appl. Mater. Interfaces* 9 (41), 36026–36037. <http://pubs.acs.org/doi/abs/10.1021/acsami.7b10768>.
- Amin, M.T., Alazba, A.A., Shafiq, M., 2015. Adsorptive removal of reactive Black 5 from wastewater using bentonite clay: isotherms, kinetics and thermodynamics. *Sustainability* 7, 15302–15318.
- Basha, C.A., Bhadrinarayana, N.S., Anantharaman, N., Meera Sheriffa Begum, K.M., 2008. Heavy metal removal from copper smelting effluent using electrochemical cylindrical flow reactor. *J. Hazard. Mater.* 152 (1), 71–78.
- Bayramoglu, M., Kobya, M., Can, O.T., Sozbir, M., 2004. Operating cost analysis of electrocoagulation of textile dye wastewater. *Sep. Purif. Technol.* 37 (2), 117–125.
- Bera, A., Kumar, T., Ojha, K., Mandal, A., 2013. Adsorption of surfactants on sand surface in enhanced oil recovery: isotherms, kinetics and thermodynamic studies. *Appl. Surf. Sci.* 284, 87–99.
- Boulinguez, B., Le Cloirec, P., Wolbert, D., 2008. Revisiting the determination of Langmuir parameters application to tetrahydrothiophene adsorption onto activated carbon. *Langmuir* 24, 6420–6424.
- Bulut, Y., Aydin, H., 2006. A kinetics and thermodynamics study of methylene blue adsorption on wheat shells. *Desalination* 194, 259–267.
- Can, O.T., Kobya, M., Demirbas, E., Bayramoglu, M., 2006. Treatment of the textile wastewater by combined electrocoagulation. *Chemosphere* 62 (2), 181–187.
- Chen, X., 2015. Modeling of experimental adsorption isotherm data. *Information* 6, 14–22. <http://www.mdpi.com/journal/information>.
- Cheung, C.W., Porter, J.F., McKay, G., 2001. Sorption kinetic analysis for the removal of cadmium ions from effluents using bone char. *Water Res.* 35, 605–612.
- Daneshvar, E., Vazirzadeh, A., Niazi, A., Kousha, M., Naushad, M., Bhatnagar, A., 2017. Desorption of methylene blue dye from brown macroalgae: effects of operating parameters, isotherm study and kinetic modeling. *J. Clean. Prod.* 152, 443–453. <http://www.sciencedirect.com/journal/journal-of-cleaner-production/vol/152/suppl/C>.

- Daneshvar, N., Ashassi Sorkhabi Kasiri, H., 2004. Decolorization of dye solution containing Acid Red 14 by electrocoagulation with a comparative investigation of different electrode connections. *J. Hazard. Mater.* 112 (1-2), 55–62.
- Dubinin, M.M., 1960. The potential theory of adsorption of gases and vapors for adsorbents with energetically non-uniform surface. *Chem. Rev.* 60, 235–266. <https://pubs.acs.org/doi/abs/10.1021/cr60204a006?journalCode=chreay>.
- Edokpayi, O., Osemwenkhae, O., Ayodele, B.V., Ossai, J., Fadilat, S.A., Ogbeide, S.E., 2018. Batch adsorption study of methylene blue in aqueous solution using activated carbons from rice husk and coconut shell. *J. Appl. Sci. Environ. Manag.* 22 (5), 631–635. <https://www.ajol.info/index.php/jasem>.
- EI-Qada, E.N., Allen, S.J., Walker, G.M., 2008. Adsorption of basic dyes from aqueous solution onto activated carbons. *Chem. Eng. J.* 135, 174.
- El-Khaiary, M.I., 2008. Least-squares regression of adsorption equilibrium data: comparing the options. *J. Hazard. Mater.* 158 (1), 73–87.
- Foo, K.Y., Hameed, B.H., 2010. Insights into the modeling of adsorption isotherm systems – a review. *Chem. Eng. J.* 156, 2–10.
- Ghaffari, H.R., Pasalari, H., Tajvar, A., Dindarloo, K., Goudarzi, B., Alipour, V., Ghanbarnejad, A., 2017. Linear and nonlinear two-parameter adsorption isotherm modeling: a case-study. *Int. J. Eng. Sci.* 6 (9), 1–11.
- Giles, C.H., Smith, D., Huitson, A., 1974. A general treatment and classification of the solute adsorption isotherm. I. Theoretical. *J. Colloid Interface Sci.* 47 (3), 755–765.
- Gnanasekaran, L., Hemamalini, R., Naushad, M., 2018. Efficient photocatalytic degradation of toxic dyes using nanostructured TiO₂/polyaniline nanocomposite. *Desalination Water Treat.* 108, 322–328. <http://www.deswater.com/doi/10.5004/dwt.2018.21967>.
- Gottipati, R., Mishra, S., 2010. Application of biowaste (Waste generated in biodiesel plant) as an adsorbent for the removal of hazardous dye – methylene blue-from aqueous phase. *Braz. J. Chem. Eng.* 27, 2.
- Gupta, G.S., Shukla, S.P., Prasad, G., Singh, V.N., 1992. China clay as an adsorbent for dye house wastewaters. *Environ. Technol.* 13, 925–936.
- Gürses, A., Doğar, Ç., Yalçın, M., Açıkyıldız, M., Bayrak, R., Karaca, S., 2006. The adsorption kinetics of the cationic dye, methylene blue, onto clay. *J. Hazard. Mater.* 131 (1), 217–228.
- Hamdaoui, O., Naffrechoux, E., 2007. Modeling of adsorption isotherms of phenol and chlorophenols onto granular activated carbon: Part II. Models with more than two parameters. *J. Hazard. Mater.* 147 (1), 401–411.

- Hameed, B.H., Ahmad, A.A., Aziz, N., 2009. Adsorption of reactive dye on palm-oil industry waste: equilibrium, kinetic and thermodynamic studies. Desalination 247 (1-3), 551–560. <https://www.sciencedirect.com/science/article/pii/S0011916409005359>.
- Ho, Y.S., Porter, J.F., McKay, G., 2002. Equilibrium isotherm studies for the sorption of divalent metal ions onto peat: copper, nickel and lead single component systems. Water Air Soil Pollut. 141 (1-4), 1–33.
- Hobson, J.P., 1969. Physical adsorption isotherms extending from ultrahigh vacuum to vapor pressure. J. Phys. Chem. 73 (8), 2720–2727.
- Idan, I.J., Luqman, C.A., Thomas, S.Y.C., Siti, N.A.B.M.J., 2018. Equilibrium, kinetics and thermodynamic adsorption studies of acid dyes on adsorbent developed from kenaf core fiber. Adsorpt. Sci. Technol. 36 (1–2), 694–712. <https://journals.sagepub.com/doi/abs/10.1177/0263617417715532>.
- Jana, S., Purkait, M.K., Mohanty, K., 2010. Removal of crystal violet by advanced oxidation and microfiltration. Appl. Clay Sci. 50, 337–341.
- Klimiuk, E., Filipkowska, U., Libecki, B., 1999. Coagulation of wastewater containing reactive dyes with the use of Polyaluminium Chloride (PAC). Pol. J. Environ. Stud. 8, 81–88. <http://www.cbr.edu.pl/eng/index.php>.
- Kooh, M.R.R., Dahri, M.K., Lim, L.B.L., 2016. The removal of rhodamine B dye from aqueous solution using *Casuarina equisetifolia* needles as adsorbent. Cogent Environ. Sci. 2, 1–14, 1140553.
- Korotkova, T.G., Ksandopulo, S.J., Donenko, A.P., Bushumov, S.A., Danilchenko, A.S., 2016. Physical properties and chemical composition of the rice husk and dust. Orient. J. Chem. 32 (6), 3213–3219.
- Kumar, K.V., 2007. Optimum sorption isotherm by linear and non-linear methods for malachite green onto lemon peel. Dyes Pigments 74 (3), 595–597.
- Kumar, K.V., Sivanesan, S., 2006. Pseudo second order kinetics and pseudo isotherms for malachite green onto activated carbon: comparison of linear and nonlinear regression methods. J. Hazard. Mater. 136, 721–726.
- Kumar, P.S., Ramakrishnan, K., Kirupha, S.D., Sivanesan, S., 2010. Thermodynamic and kinetic studies of cadmium adsorption from aqueous solution onto rice husk. Braz. J. Chem. Eng. 27 (2), 347–355.
- Lagergren, S., 1898. About the theory of so-called adsorption of soluble substances. K. Sven. Vetenskapsakad. Handl. 24 (4), 1–39.

- Lakshmi, U.R., Srivastava, V.C., Mall, I.D., Lataye, D.H., 2009. Rice husk ash as an effective adsorbent: evaluation of adsorptive characteristics for Indigo Carmine dye. *J. Environ. Manag.* 90, 710–720.
- Langmuir, I., 1918. The adsorption of gases on plane surfaces of glass, mica and platinum. *J. Am. Chem. Soc.* 40, 1361–1403.
- Liang, Z., Wang, Y.X., Zhou, Y., Liu, H., 2009. Coagulation removal of melanoidins from biologically treated molasses wastewater using ferric chloride. *Chem. Eng. J.* 152 (1), 88–94.
- Lin, S.H., Peng, C.F., 1994. Treatment of textile wastewater by electrochemical method. *Water Res.* 28 (2), 277–282.
- Lodha, S., Jain, A., Punjabi, P.B., 2011. A novel route for waste water treatment: photocatalytic degradation of rhodamine B. *Arab. J. Chem.* 4, 383–387.
- Mahalakshmi, M., Arabindoo, B., 2007. Photocatalytic degradation of carbofuran using semiconductor oxides. *J. Hazard. Mater.* 143, 240–245. PMID: 17045739.
- Maldonado, M., Malato, S., Perez-Estrada, L., 2006. Partial degradation of five pesticides and an industrial pollutant by ozonation in a pilot-plant scale reactor. *J. Hazard. Mater.* 38, 363–369.
- Marquardt, D.W., 1963. An algorithm for least-squares estimation of nonlinear parameters. *J. Soc. Ind. Appl. Math.* 11, 431–441. <http://www.sciencedirect.com/science/article/pii/0022283363704536>.
- Martin, M., Perez, J., 2008. Degradation of alachlor and pyrimethanil by combined photo- fenton and biological oxidation. *J. Hazard. Mater.* 15 (5), 342–349.
- Meghea, A., Rehner, H., 1998. Test-fitting on adsorption isotherms of organic pollutants from waste waters on activated carbon. *J. Radioanal. Nucl. Chem.* 229 (1-2), 105–110.
- Ming-Twanga, S., Zaini, M.A.A., Salleh, L.M., Yunus, M.A.C., Naushad, M., 2017. Potassium hydroxide-treated palm kernel shell sorbents for the efficient removal of methyl violet dye. *Desalination Water Treat.* 84, 262–270. <http://www.deswater.com/doi/10.5004/dwt.2017.21206>.
- Mohan, N., Balasubramanian, N., Basha, C.A., 2007. Electrochemical oxidation of textile wastewater and its reuse. *J. Hazard. Mater.* 147 (1-2), 644–651.
- Murthy, H., Manonmani, H., 2007. Aerobic degradation of technical hexachlorocyclohexane by a defined microbial consortium. *J. Hazard. Mater.* 149, 18–25.
- Nandi, B.K., Goswami, A., Purkait, M.K., 2009. Adsorption characteristics of brilliant green dye on kaolin. *J. Hazard. Mater.* 161, 387–395.

- Nandi, B.K., Patel, S., 2017. Effects of operational parameters on the removal of brilliant green dye from aqueous solutions by electrocoagulation. *Arab. J. Chem.* 10, 2961–2968.
- Naushad, M., Ahamad, T., Al-Maswari, B.M., Alqadami, A.A., Alshehri, S.M., 2017. Nickel ferrite bearing nitrogen-doped mesoporous carbon as efficient adsorbent for the removal of highly toxic metal ion from aqueous medium. *Chem. Eng. J.* 330, 1351–1360.
- Naushad, M., Alothman, Z.A., Awual, M.R., Ahamad, T., 2016. Adsorption of rose Bengal dye from aqueous solution by amberlite Ira-938 resin: kinetics, isotherms and thermodynamic studies. *Desalination Water Treat.* 57 (29), 13527–13533. <http://www.tandfonline.com/doi/abs/10.1080/19443994.2015.1060169>.
- Ncibi, M.C., 2008. Applicability of some statistical tools to predict optimum adsorption isotherm after linear and non-linear regression analysis. *J. Hazard. Mater.* (153), 207–212.
- Ng, J.C.Y., Cheung, W.H., McKay, G., 2002. Equilibrium studies of the sorption of Cu(II) ions onto chitosan. *J. Colloid Interface Sci.* 255, 64–74.
- Ng, J.C.Y., Cheung, W.H., McKay, G., 2003. Equilibrium studies for the sorption of lead from effluents using chitosan. *Chemosphere* 52, 1021–1030.
- Nouri, L., Ghodbane, I., Hamdaoui, O., Chiha, M., 2007. Batch sorption dynamics and equilibrium for the removal of cadmium ions from aqueous phase using wheat bran. *J. Hazard. Mater.* 149, 115–125.
- Panahi, R., Vasheghani-Farahani, E., Shojasadati, S., 2008. Determination of adsorption isotherm for l-lysine imprinted polymer. *Iran. J. Chem. Eng.* 5 (4), 49–55. <https://scholar.google.com/citations?user=78ijOqcAAAAJ&hl>.
- Pathania, D., Sharma, G., Kumar, A., Naushad, M., Kalia, S., Sharma, A., Alothman, Z.A., 2015. Combined sorptional-photocatalytic remediation of dyes by polyaniline Zr(IV) selenotungstophosphate nanocomposite. *Toxicol. Environ. Chem.* 97 (5), 526–537. <http://www.tandfonline.com/doi/full/10.1080/02772248.2015.1050024?scroll=top&ne edAccess=true>.
- Piccin, J.S., Dotto, G.L., Pinto, L.A.A., 2011. Adsorption isotherms and thermochemical data of Fd&C red N° 40 binding by chitosan. *Braz. J. Chem. Eng.* 28 (2), 295–304.
- Ponnusami, V., Vikram, S., Srivastava, S.N., 2008. Guava (*Psidium guaiava*) leaf powder: novel adsorbent for removal of methylene blue from aqueous solutions. *J. Hazard. Mater.* 152, 276–286.

- Purkait, M.K., DasGupta, S., De, S., 2003. Removal of dye from wastewater using micellar-enhanced ultrafiltration and recovery of surfactant. *Sep. Purif. Technol.* 37, 81–92.
- Rahman, M.S., Sathasivam, K.V., 2015. Heavy metal adsorption onto *Kappaphycus* sp. from aqueous solutions: the use of error functions for validation of isotherm and kinetics models. *BioMed Res. Int.* 1–13. Article ID 126298.
- Ramuthai, S., Nandhakumar, V., Thiruchelvi, M., Arivoli, S., Vijayakumaran, V., 2009. Rhodamine B adsorption-kinetic, mechanistic and thermodynamic studies. *E J. Chem.* 6 (1), 363–373.
- Redlich, O., Peterson, D.L., 1959. A useful adsorption isotherm. *J. Phys. Chem.* 63 (6), 1024.
- Sharma, G., Naushad, M., Kumar, A., Rana, S., Khan, M.R., 2017. Efficient removal of coomasie brilliant blue R-250 dye using starch/poly(alginic acid-*cl*-acrylamide) nanohydrogel. *Process Saf. Environ. Protect.* 109, 301–310.
- Shelke, R., Jagdish, B., Balaji, M., Milind, U., 2010. Adsorption of acid dyes from aqueous solution onto the surface of acid activated Nirgudi Leaf powder (AANLP): a case study. *Int. J. ChemTech Res.* 2 (4), 2046–2051.
- Shirmardi, M., Mesdaghinia, A., Mahvi, A.H., Nasser, S., Nabizadeh, R., 2012. Kinetics and equilibrium studies on adsorption of acid red 18 (Azo-dye) using multi-wall carbon nanotubes (MWCNTs) from aqueous solution. *E J. Chem.* 9 (4), 2371–2383.
- Sips, R., 1948. On the structure of a catalyst surface. *J. Chem. Phys.* 16, 490–495.
- Srivastava, V.C., Swamy, M.M., Mall, I.D., Prasad, B., Mishra, I.M., 2006. Adsorptive removal of phenol by bagasse fly ash and activated carbon: equilibrium, kinetics and thermodynamics. *Colloids Surf. Physicochem. Eng. Aspects* 272 (1-2), 89–104.
- Subramanyam, B., Das, A., 2009. Comparison of linearized and non-linearized isotherm models for adsorption of aqueous phenol by two soils. *Int. J. Environ. Sci. Technol.* 6, 633–640.
- Subramanyam, B., Das, A., 2014. Linearised and non-linearised isotherm models optimization analysis by error functions and statistical means. *J. Environ. Health Sci. Eng.* 12 (1), 92–101. PMCID: PMC4091749. PMID: 25018878.
- Tahir, H., Hammed, U., Sultan, M., Jahanzeb, Q., 2010. Batch adsorption technique for the removal of malachite green and fast green dyes by using montmorillonite clay as adsorbent. *Afr. J. Biotechnol.* 9, 8206–8214. <http://www.academicjournals.org/AJB>.

- Tehrani-Bagha, A.R., Nikkar, H., Mahmoodi, N.M., Markazi, M., Menger, F.M., 2011. The sorption of cationic dyes onto kaolin: kinetic, isotherm and thermodynamic studies. *Desalination* 266 (1), 274–280.
- Temkin, M.J., Pyzhev, V., 1940. Kinetics of the synthesis of ammonia on promoted iron catalysts. *Acta Physicochim.* 12, 217–222. www.sciepub.com/reference/163926.
- Thompson, G., Swain, J., Kay, M., Forster, C.F., 2001. The treatment of pulp and paper mill effluent: a review. *Bioresour. Technol.* 77 (3), 275–286.
- Toth, J., 1971. State equations of the solid gas interface layer. *Acta Chem. Acad. Hung.* 69, 311–317. <http://www.oalib.com/references/8716521>.
- Venkatesh, R., Amudha, T., Sivaraj, R., Chandramohan, M., Jambulingam, M., 2010. Kinetics and equilibrium studies of adsorption of direct red-28 onto *Punica granatum* carbon. *Int. J. Eng. Sci. Technol.* 2 (6), 2040–2050.
- Vijayaraghavan, K., Padmesh, T.V.N., Palanivelu, K., Velan, M., 2006. Biosorption of nickel(II) ions onto *Sargassum wightii*: application of two-parameter and three-parameter isotherm models. *J. Hazard. Mater.* 133 (1-3), 304–308.
- Wang, L., Zhang, J., Zhao, R., Li, Y., Li, C., Zhang, C., 2010. Adsorption of Pb(II) on activated carbon prepared from *Polygonum orientale* Linn.: kinetics, isotherms, pH, and ionic strength studies. *Bioresour. Technol.* 101 (15), 5808–5814.
- Zafar, S.I., Bisma, M., Saeed, A., Iqbal, M., 2008. FTIR spectrophotometry, kinetics and adsorption isotherms modelling, and SEM-EDX analysis for describing mechanism of biosorption of the cationic basic dye Methylene blue by a new biosorbent (Sawdust of Silver Fir; *Abies Pindrow*). *Fresen. Environ. Bull.* 17, 2109–2121. www.google.com/amp/s/www.researchgate.net/publication/252932859.
- Zhu, Y.N., Wang, D.Q., Zhang, X.H., Qin, H.D., 2009. Adsorption removal of methylene blue from aqueous solution by using bamboo charcoal. *Fresen. Environ. Bull.* 18, 369–376. <https://www.researchgate.net/publication/286339451>.